Responses and Injuries of Male Post-Mortem Human Subjects (PMHS) Seated in an Unreinforced Production Seat in Rear-facing Frontal Impacts

Yun-Seok Kang, Tim DeWitt, Angelo Marcallini, Jiwoon Song, Yong Hyun Jung, Dong Gil Lee, Jae Jun Harm, Seokhoon Ko, Hyung Joo Kim, Randee Hunter, Gretchen Baker, Amanda M. Agnew

Abstract This study investigated male post-mortem human subject (PMHS) responses and injuries using an unreinforced production seat in rear-facing frontal impacts. Two PMHS were tested at ΔV of 56kph in an unreinforced production seat with a pretensioner in upright and reclined seatback angles. PMHS were positioned using the same procedures as in a previous study. An instrumented panel was installed behind the seatback with a gap of 100mm that limited seatback rotation. PMHS instrumentation was identical to those used in the previous study with additional strain rosettes on the ribs and strain gauges on the superior pubic rami of the pelves. The major PMHS injuries occurred in the thorax and spine. Both PMHS sustained critical rib fractures (AIS5) and serious to maximal cervical spine injuries (AIS3-6). All rib fractures occurred before maximum seatback rotation. Posterior rib principal strain directions were in an upward direction, indicating shear in the thorax. Both PMHS sustained cervical and thoracic spine injuries due to excessive ramping-up motion. No pelvis fractures occurred, but fibula fractures were observed which suggests more energy was transferred to the lower extremity than in previous tests. The results from this study can be utilised for designing rear-facing seats in vehicles with automated driving systems.

Keywords Alternative seat configuration, neck hyperextension, thorax injury, rib fracture, seatback rotation

I. INTRODUCTION

Non-standard seating configurations are likely to be used with the emergence of vehicles with an automated driving system (ADS) [1-2]. As these vehicles merge into the fleet currently being driven by humans on roads, vehicle-to-vehicle impacts will undoubtedly continue to occur, at least in the near term. Given that occupants are not required to drive when using vehicles with an ADS, one potential alternative seating configuration proposed in consumer preference studies, particularly considering long-distance travel with children and seniors, is a rear-facing configuration [2-4]. However, due to a lack of field crash data as well as biomechanical data in rear-facing scenarios, evaluating the protection of passengers in the event of an impact has become a new challenge for both the biomechanics and crashworthiness research fields. In addition, current safety tools, such as anthropomorphic test devices (ATDs) and human body models (HBMs), have not been designed and optimised for the rear-facing configuration. Therefore, biomechanical responses and injuries of post-mortem human subjects (PMHS) in rear-facing configurations should be investigated to enhance safety tools and seat design.

There are a few studies focused on the biomechanical responses and injuries of PMHS seated in both upright and reclined seats in high-speed (ΔV 56km/h) rear-facing frontal impacts (HSRFFI) [5-6]. In these previous studies, original equipment manufacturer (OEM) seats, such as a 2018 Honda Odyssey with an All-Belt-To-Seat (ABTS condition) and 2018 Honda Accord with Fixed D-Ring (FDR condition), were evaluated with two different recline angles (25deg and 45deg). The seatback and head restraint were rigidly reinforced to ensure repeatability and durability of the seat and sled system during the events. Biomechanical responses for the head, thorax, pelvis, and lower extremity were provided to help improve ATDs and HBMs for use in HSRFFI scenarios. PMHS injuries included ligament damage to the cervical spine, upper extremity injuries, rib fractures, pelvis fractures, and lower extremity injuries. The major injuries sustained by the PMHS were rib and pelvis fractures. Given that the posterior thorax directly interacts with the seatback in rear-facing conditions, one of the factors that might

Y-S. Kang is an Associate Professor (tel: +1 614 366 7584, e-mail: yunseok.kang@osumc.edu), T Dewitt, A Marcallini, R Hunter, G Baker, and A Agnew are with the Injury Biomechanics Research Center at The Ohio State University, USA. J Song, YH Jung, DG Lee, JJ Harm, and S Ko are with Hyundai Mobis Co., Ltd, in Gyeonggi-do, Korea. HJ Kim is at Hyundai Motor Company, in Gyeonggi-do, Korea.

influence the likelihood of sustaining rib and pelvis fractures is the structural properties of the OEM seats, which were not designed for protecting occupants in HSRFFI conditions but instead for mitigating neck injuries in low-speed rear-ended impacts (ΔV<17km/h). The number of rib fractures (NRF) and number of fractured ribs (NFR) were greater in the FDR condition than the ABTS condition regardless of recline angle. All PMHS tested in the FDR condition regardless of recline angle sustained pelvis fractures, while four out of six PMHS tested in the ABTS condition did not sustain pelvis fractures, indicating that different seat structures and properties could affect PMHS thoracic responses and injury outcomes in these reinforced seatback scenarios [7].

Rear-facing frontal impact conditions are not equivalent to high-speed rear impacts due to the differences in energy dissipation mechanisms between front compartments, e.g., front bumper and engine compartment, and rear compartments, e.g., rear bumper and trunk, [8]. Moreover, the literature regarding thoracic injuries and rib fractures resulting from high-speed rear impacts is scarce but should be considered to learn more about possible injury causation. Previous studies using crash databases, such as National Automotive Sampling System-Crashworthiness Data System (NASS-CDS) and German In-Depth Accident Study (GDAS), found that thoracic injuries, such as rib fractures, are common in high-speed rear impact cases [9-10]. Viano and Parenteau [9] found that serious thoracic injuries occurred in moderate-to-high speed rear impacts at ΔV ranging from 18 to 73km/h. They identified seatback interaction with occupants due to high energy being transferred to the seat as a source of thoracic injuries [9]. Zellmer et al. [10] identified cases involved in high-speed rear-impact crashes from 1999 to 2017 (ΔV ranging from 26 – 91km/h) in which occupants sustained rib fractures [10]. Although these crash database studies provide valuable insights on rib fractures in high-speed rear impacts, the influence of seatback structure and response, i.e., seat strength related to yielding seatback or high-retention seatback, on rib fracture risk remains unknown.

To understand the effect of seatback rotation on occupant response and injury risk in HSRFFI, a finite element (FE) HBM, e.g., Total Human Model for Safety (THUMS), seated in a publicly available FE production seat model, which simulated rotational and yielding seatback (referred to as a compliant seat in the study), was utilised in a previous FE modelling study [11]. A rigid seatback was also modelled by applying an extreme stiffness to the seat frame and recliner while maintaining all other seat properties (same geometry, seat foam, seat cover, etc.). Two different recline angles (23 and 45deg) and three different speeds (24, 40, and 56kph) were used to explore influences of these variables on the THUMS response and injury metrics. A rotational and yielding seatback was found to reduce neck injury values, but brain and chest injury metrics were higher than those from the rigid seat condition. Although the THUMS model has not been validated in severe rear-facing impacts, this previous study provided valuable insights into possible injury trends affected by seatback rotational stiffness (compliant vs. rigid).

Therefore, this study aimed to investigate responses and injuries of male PMHS seated in an unreinforced, i.e., yielding and rotating seatback, production seat during HSRFFI at the same sled speed (ΔV 56kph) as the previous rear-facing PMHS studies [5-7] for comparison.

II. METHODS

Sled Setup

An original equipment manufacturer (OEM) seat (2022 Hyundai Staria second-row seat) equipped with an integrated seat belt (or all-belt-to-seat) was mounted on a Hydraulic-controlled Gas-Energized (HyGE) sled to simulate rear-facing frontal impacts (Fig. 1). The belt retractor was attached to the seatback frame, while the buckle and anchor were installed on the seat pan frame. The retractor was also equipped with a pretensioner that was activated at 12ms. Two recline conditions (upright: manufacturer design seatback angle and relaxed: upright + 20deg) were used in this study. A general overview of the PMHS sled setup is presented in Fig. 1. Three seat belt tension load cells (EL20-5458, TE connectivity, Berwyn, PA, USA) were attached to the belt webbing to measure tension of the shoulder and lap belts. One shoulder belt and two lap belt load cells were used for PMHS A. However, since the two lap belt loads were very similar in PMHS A, the left side lap belt load cell was moved to the lower shoulder belt in the second test, so two shoulder belts and one lap belt were utilised for PMHS B. To mimic more realistic vehicle boundary conditions than those used in the previous studies [5-7] and prevent seatback collapse during events, an instrumented panel (IP) was also incorporated into the sled setup. The distance between the back of the seatback and front of the IP was maintained at 100mm for both recline angles (Fig. 1). Two sets of conductive adhesive tape were attached to the back centre and back left side of the seatback

and the front of the IP to quantify seatback-to-IP contact timing (Fig. A1). The same sled pulse used in the previous rear-facing studies [5-6] was applied to a HyGE sled system at ΔV of 56km/h (Fig. A2). Sixteen motion capture cameras (Vantage 5, VICON, Hauppauge, NY, USA) were placed surrounding the sled to visualise photo reflective markers installed on the sled, seat, and PMHS to quantify seat deformation and PMHS kinematics. VICON data were captured at 1,000 Hz and aligned to the SAE J211 coordinate system [12].

(a) PMHS A in upright condition

(b) PMHS B in relaxed condition

Fig.1. General sled setup

PMHS Characteristics

The Ohio State Body Donation Program Advisory Committee, USA, the internal ethics committee for the use of PMHS in research, approved the use of PMHS from The Ohio State University Body Donation Program for this study. Characteristics for PMHS (n=2) tested in this study and those previously tested in [7] are provided in Table I. PMHS A was 79 years old, and PMHS B was 70 years old, which was older than the average PMHS age (61 ± 5years) from the previous study [7]. Heights (166.5cm for PMHS A, 165.4cm for PMHS B) were slightly shorter than the previous study (176.0 ± 4.8cm), while weights (84.1kg for PMHS A, 70.5kg for PMHS B) were comparable to those in the previous study (80.0 ± 12.7kg). Seated height for PMHS A (86.9cm) was shorter than the previous average seated height (94.3 ± 2.3cm), while seated height for PMHS B (92.2cm) was comparable to the previous study [7]. Dual-energy x-ray absorptiometry (DXA) was used to quantify areal bone mineral density (aBMD). The lumbar spine aBMD T-score (2.7 and 1.7) for PMHS tested in this study was slightly higher than the average (0.2 ± 1.3) in [7], but all were in the normal range (Table I). Detailed anthropometric measurements are provided in Table BI.

TABLE I
PMHS CHARACTERISTICS

	Sex	Age (yr)	Height (cm)	Weight (kg)	Seated height (cm)	aBMD L2-L4 T-score
PMHS A	M	79	166.5	84.1	86.9	2.7
PMHS B	M	70	165.4	70.5	92.2	1.7
Mean (SD), n=14 in [7]	M	61 (5)	176.0 (4.8)	80.0 (12.7)	94.3 (2.3)	0.2 (1.3)

PMHS Instrumentation

PMHS instrumentation techniques and types used in this study were consistent with the previous studies [5-6], but additional instrumentation was used (Table II and Fig. A3). Four additional strain rosette gauges (CEA-06-062UR-350/P2, Micro Measurements, Wendell, NC, USA) were attached posteriorly on the 6th and 7th ribs to quantify principal strains and their directions. Additionally, uniaxial strain gauges (CEA-13-062UW-350/P2, Micro Measurements, Wendell, NC, USA) were added to the superior pubic rami and right clavicle (PMHS B only) to identify possible fractures. VICON markers were attached to each body region to quantify the overall kinematics

of the PMHS during the events. Due to space limitations, results from some body regions will not be discussed in this manuscript.

Whole body computed tomography (CT) scans with a slice thickness of 0.6mm and scan parameters of 120kVp and 250mAs were obtained for each PMHS to locate any pre-existing abnormalities and injuries (pre-test CT), document instrumentation position and orientation (instrumentation CT), and identify injuries after sled tests (post-test CT).

TABLE II
PMHS INSTRUMENTATION

Anatomical Site	Instrumentation Type
Head	6aω installed on a tetrahedron fixture
Clavicle	Uni-axial strain gage at R clavicle* (PMHS B only)
Humerus	6DOF motion block and uni-axial strain gage at R and L mid-shaft humerus
C4, T1, T4, T8, T12, and S1	6DOF motion blocks
Chest	59 channel chestband (mid-sternum)
Ribs	Uni-axial strain gages: - R and L ribs 3 - 9 on anterior aspect - R and L ribs 3 - 4 and 7 - 10 on posterior aspect Strain rosettes*: - R and L ribs 6 and 7 on posterior aspect
Pelvis	6DOF motion block at R and L iliac wing Uni-axial strain gages*: - R and L superior pubic rami
Femur and Tibia	6DOF motion block and uni-axial strain gage at R and L mid-shaft femur and tibia

* additional instrumentation not included in [5-6]. R = right, L = left

PMHS Positioning

The PMHS seating procedure was consistent with the previous studies [5-6]. The pelvis and lumbar spine region of the PMHS were pushed against the seatback to reduce the possible gap between the PMHS and the seatback. While the mid-sagittal plane of the PMHS was aligned with the centreline of the seatback, the upper torso and head were aligned to the centreline of the seatback and head restraint, respectively. The PMHS was positioned using a regression model determined from a volunteer seating study [13]. The PMHS positioning targets and corresponding measured values are provided in Table BII. Although great effort was made to achieve the positioning targets, the head angle for PMHS B could not be achieved, likely due to differences in seat and head restraint geometries between the seat used in the current study compared to the one used in [13]. Initial belt tensions consistent with the previous studies [5-6] (26.7N lap belt and 17.8N shoulder belt) were applied to the seat belt. PMHS skeletal position and orientation including spine curvatures were visualised using X-ray images obtained from a portable digital X-ray device (Mobile X-ray EPX-F2800, Ecotron, Seoul, South Korea) with the PMHS seated (Fig. B2). Point digitisation and 3D surface scans were performed to obtain 3D coordinates for body landmarks, instrumentation locations and orientations, and overall PMHS posture (Fig. B3) using a FARO arm device (Edge FaroArm, Faro Arm Technologies, Lake Mary, FL, USA). The seat was replaced for each sled test.

Data Collection and Analysis

A KT data acquisition system (Kayser-Threde, Munich, Germany) collected data channels from the sled (sled acceleration) and seat belt tension load cells. All PMHS data channels were recorded using a DTS data acquisition system (SLICE PRO, DTS, Seal Beach, CA, USA). Both KT and DTS data acquisition systems were operated using 20,000 samples per second. Five high-speed cameras (three on-board and two off-board cameras) recorded the general PMHS kinematics at 1,000 frames per second. Identical SAE J211 filtering classes to those used in [5] were

utilised in this study. The accelerometer and angular rate sensor data were transformed to the anatomical origins and coordinate systems used in the previous studies [5-6]. The chest band data were processed using a custom MATLAB post-processing script (Crashstar, NHTSA) to calculate anterior-to-posterior (A-P) chest deflections at the level of mid-sternum. Rib fracture timing was identified using the strain and strain rate method proposed by [7]. Principal strain and angle with respect to the strain rosette coordinate system were calculated using strain rosette equations, Equations 1 and 2, respectively. Principal strain magnitudes and angles measured at left and right posterior 6th and 7th ribs (L6, R6, L7, and R7) were overlaid with rib orientation photos taken immediately after the strain rosette placement on the ribs.

$$\epsilon_{P,Q} = \frac{\epsilon_1 + \epsilon_3}{2} \pm \sqrt{\frac{(\epsilon_1 - \epsilon_2)^2 + (\epsilon_2 - \epsilon_3)^2}{2}} \quad (1)$$

$$\Phi_{P,Q} = \frac{1}{2}\tan^{-1}\left(\frac{2\epsilon_2 - \epsilon_1 - \epsilon_3}{\epsilon_1 - \epsilon_3}\right) \pm \sqrt{\frac{(\epsilon_1 - \epsilon_2)^2 + (\epsilon_2 - \epsilon_3)^2}{2}} \quad (2)$$

where, $\epsilon_{P,Q}$ are maximum and minimum principal strains. ϵ_1, ϵ_2 and ϵ_3 are strain measured at each axis shown in Fig. B4. $\Phi_{P,Q}$ are mean angles of the maximum and minimum principal stains.

PMHS kinematics obtained from the current study were compared to those from the previous study [5], in which six PMHS were tested in a reinforced Honda Odyssey seat equipped with ABTS using two different recline angles (25deg: ABTS25, N=3 and 45deg: ABTS45, N=3) at ΔV of 56kph (the same sled input).

Following each PMHS sled test, a detailed whole-body dissection was performed to document injuries induced by the sled tests. A Certified Abbreviated Injury Scale (AIS) [14] Specialist (CAISS) classified all skeletal and soft tissue injuries.

III. RESULTS

Injury Outcomes

A summary of PMHS injuries is provided in Table III. Both PMHS sustained a critical number and distribution of rib fractures resulting in bilateral flail chest (AIS5). The number of rib fractures (NRF) for PMHS A and PMHS B were 32 and 27, while the number of fractured ribs (NFR) were 21 and 18 for PMHS A and PMHS B, respectively. PMHS A and PMHS B also both sustained massive pneumothoraces (AIS5). Both PMHS sustained thoracic and cervical spine injuries as well. For the thoracic spine, PMHS A sustained a complete spinal cord transection with bilateral dislocation and fracture at T4 (AIS5), while PMHS B sustained a major vertebral body fracture at T1 (AIS3). In the cervical spine, PMHS A sustained a complete spinal cord transection with bilateral dislocation and fracture at C1 (AIS6). PMHS B sustained bilateral dislocation with disc rupture at C2 (AIS3). Both PMHS sustained right distal clavicle fractures (AIS2) and proximal fibula fractures (AIS2) on the left and right for PMHS B and on the left only for PMHS A. Injuries to PMHS A resulted in a maximum AIS (MAIS) of 6 and an Injury Severity Score (ISS) of 75, while injuries to PMHS B resulted in a MAIS of 5 and ISS of 38.

Seat and Restraint Responses

Seatbelt loads are presented in Fig. 2. For PMHS A, both lap belt loads (3685N for left lap belt, 3557N for right lap belt) were greater than the shoulder belt (2419N). Since both left and right lap belt loads were consistent, the left lap belt tension load cell was moved to the shoulder belt close to the buckle (bottom shoulder belt) for PMHS B (Fig. 1). The first peak from the shoulder belts occurred around 16ms due to the pretensioner being activated at 12ms. For PMHS B, the bottom shoulder belt load (4449N) was higher than the top shoulder belt (2446N) and right lap belt (3816N) loads. Time histories for the seatback-to-IP contact switches are provided in Fig. C1. The seatback began to contact the IP at 52.4ms (centre) for PMHS A and 49.6ms (left) for PMHS B and separated from the IP at 137.4ms (centre) for PMHS A and 118.95ms (left) for PMHS B. PMHS A seatback contacted the IP later than PMHS B due to the difference in recline conditions (upright vs. relaxed). Peak seatback rotation calculated from VICON markers were 38.1deg at 78.0ms for PMHS A and 25.7deg at 74ms for PMHS B. Sequential seatback motions and whole-body kinematics for each PMHS are provided in Fig. C2 and Fig. C3.

TABLE III
PMHS INJURY SUMMARY

	Body Region	AIS code	Description
PMHS A	Manubrium	450804.2	e
	Rib	450214.5	Bilateral flail chest Number of rib fractures: 32 Number of fractured ribs: 21 L ribs: L1, L2, L3, L4, L5, L6, L7, L8, L9, L10 (flail ribs: L3-L7) R ribs: R1, R2, R3, R4, R5, R6, R7, R8, R9, R10, R11 (flail ribs: R2-R5)
		442204.5	Pneumothorax: @ L3-L5, R4-R5 (equiv. to massive air leak)
	Thoracic spine	650420.1	Transverse process fracture: T1R
		650417.2	Bilateral transverse process fractures (multiple of same vertebra) T2L&R, T3L&R, T4L&R, T5L&R, T6L&R
		650418.1	Spinous process fracture: T9
		610428.5	T4/T5: complete spinal cord transection with bilateral dislocation and fracture (only posterior longitudinal ligament was connected)
	Cervical spine	610236.6	C1/C2: complete spinal cord transection with bilateral dislocation and fracture
		650232.2	C5: inferior end plate fracture (minor compression)
		650205.3	C5/C6: complete disc rupture
		650299.2	C6/C7: disc injury (NSF)
	Upper extremity	750761.2	Right distal clavicle fracture (intra-articular)
	Lower extremity	854471.2	Left proximal fibula fracture
PMHS B	Rib	450214.5	Bilateral flail chest Number of rib fractures: 27 Number of fractured ribs: 18 Left ribs: L1, L2, L3, L4, L5, L6, L7, L10, L11 (flail ribs: L2-L6) Right ribs: R1, R2, R3, R4, R5, R6, R7, R8, R9 (flail ribs: R3-R5)
		442204.5	Pneumothorax: @ L4-L5 (equiv. to massive air leak)
	Thoracic spine	650420.1	Transverse process fracture: T1L, T4L, T5L, T6L
		650417.2	Bilateral transverse process fractures (multiple of same vertebrae): T2L&R
		650434.3	T1 major vertebral body fracture (spinal cord intact)
	Cervical spine	650212.3	C2/C3 bilateral dislocation (spinal cord intact, dura damaged)
		650205.3	C2/C3 disc rupture
		610220.1	Transverse process fracture: C3L
	Upper extremity	750751.2	Right distal clavicle fracture (extra-articular)
	Lower extremity	854471.2	Left proximal fibula fracture
		854471.2	Right proximal fibula fracture

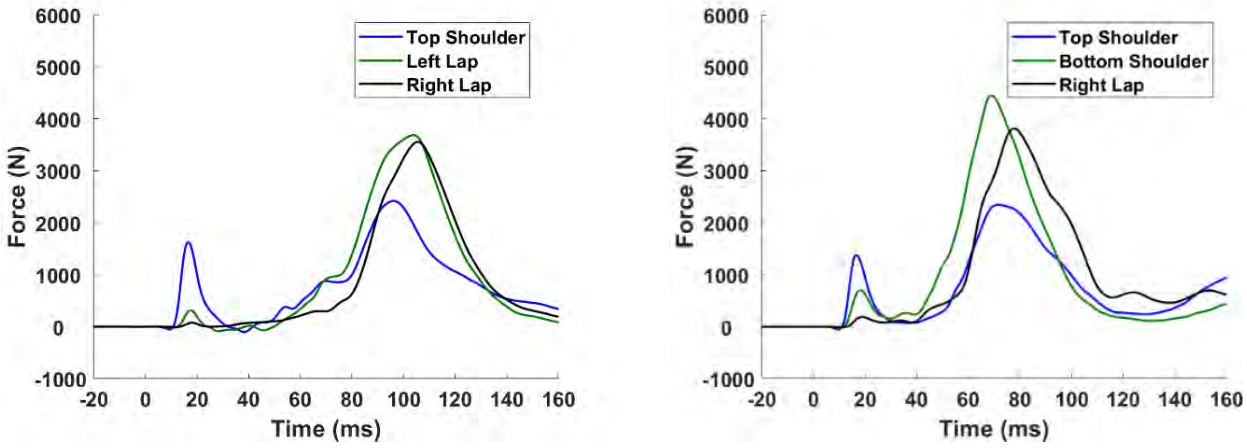

(a) PMHS A (b) PMHS B

Fig. 2. Seat belt loads

Head and T1 Kinematics

Linear and angular kinematics measured from the head and T1 are shown in Fig. 3. Since the unreinforced seatback used in this study rotated rearward, head and T1 x-accelerations became smaller than average acceleration measured from the reinforced ABTS conditions (Figs. 3a and 3b). However, since the PMHS experienced hyperextension (Figs. 3e, C2, and C3), z-accelerations were greater than in the ABTS conditions. The head local z-axis was aligned to the main sled moving direction, due to large rearward head rotations (135.2deg for PMHS A and 85.0deg for PMHS B). Regardless of recline angle, head and T1 angular velocity and rotation about the y-axis were remarkably greater than those from the ABTS conditions (Figs 3c, 3d, 3e, and 3f). Time histories are provided in Figs. C4 (head) and C5 (T1). Head contact timing measured for PMHS A was 62.6ms. However, for PMHS B, the head was initially in contact with the head restraint to mimic a relaxed occupant position.

T4, T8, and T12 Kinematics

Peak linear and angular kinematics at T4, T8, and T12 are presented in Fig. C6. T4 kinematics exhibited similar trends as T1. T4 x-accelerations for PMHS A and PMHS B were lower than the average acceleration obtained from the ABTS conditions, while the opposite trend was observed for z-acceleration. T4 y-angular velocities were greater than in the ABTS conditions, particularly with PMHS A, tested in the upright condition (Fig. C6d). For T8 and T12, linear x-accelerations from PMHS A were lower than ABTS25, while those from PMHS B were comparable to ABTS45. However, z-accelerations were slightly lower than those from the ABTS conditions (Figs. C6a, C6b, and C6c). No clear trends were found in the peak y-angular velocities. Time history plots are also provided in Figs. C7 – C9.

Thoracic Responses

Anterior-to-posterior (A-P) chest deflections determined from the chestband are shown in Fig. 4. Maximum A-P chest deflections were 27.7mm (18.7% @ 57.65ms) for PMHS A and 30.7mm (25.8% @ 61.60ms) for PMHS B. Rib fractures identified by strain and strain rate signals are provided in Fig. 5. Rib fractures occurred between 61.55ms and 68.80ms for PMHS A and 51.3ms to 72.35ms for PMHS B. Corresponding PMHS kinematics to rib fracture start and end timings are shown in Fig. 6. Maximum principal strains and angles that were computed from the strain rosettes on the posterior of 6th and 7th ribs are provided in Fig. C10. The thorax experienced oblique directions of maximum principal strains (Fig. C10a) when the anterior rib fracture occurred at the right 6th rib for PMHS A. These principal strain directions were likely induced by rib bending caused by the A-P chest compression and rib shear due to inferior-to-superior (I-S) thoracic deformation. However, for PMHS B, the posterior of right 6th and 7th ribs experienced oblique directions of maximum principal strains, while the principal strain directions from the left were longitudinal to the main rib axis (or along the rib

direction). When the maximum principal direction was close to being aligned along the rib longitudinal axis, the principal strain magnitudes (left 6th and 7th ribs in Fig. C10) were much higher than those from oblique principal strain directions (right 6th and 7th ribs in Fig. C10).

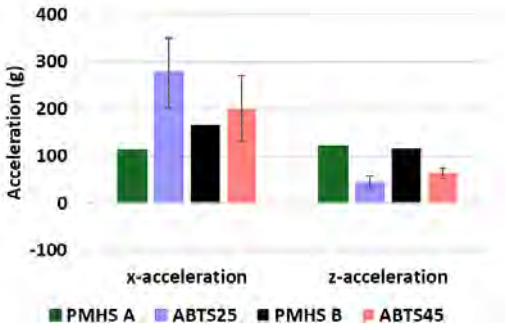

(a) Head linear acceleration

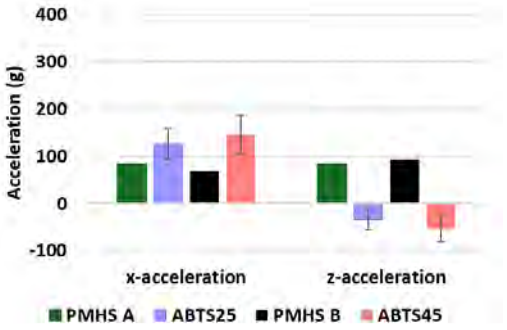

(b) T1 linear acceleration

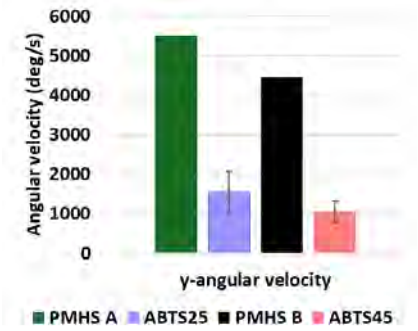

(c) Head angular velocity about y-axis

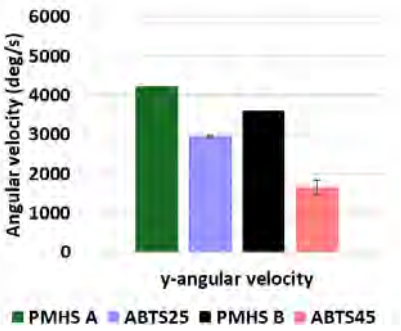

(d) T1 angular velocity about y-axis

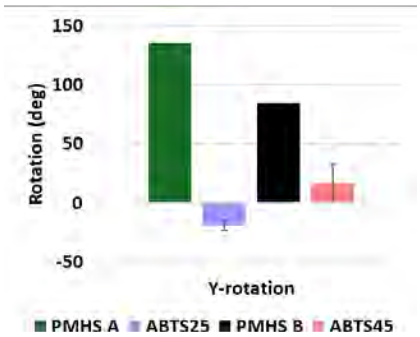

(e) Head rotation about Y-axis

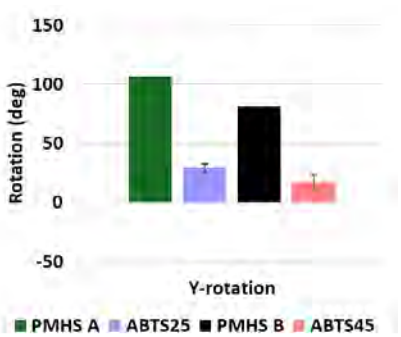

(f) T1 rotation about Y-axis

Fig. 3. Head and T1 kinematics

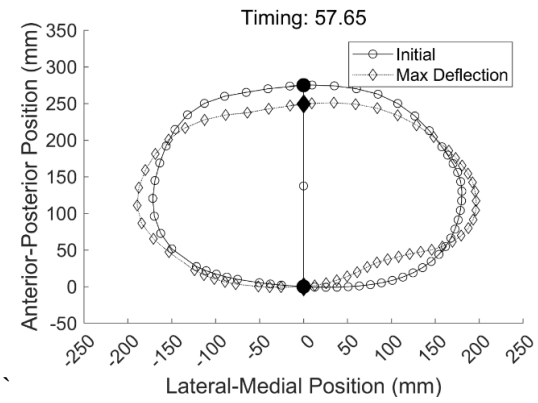

(a) PMHS A (25.7mm, 18.7%)

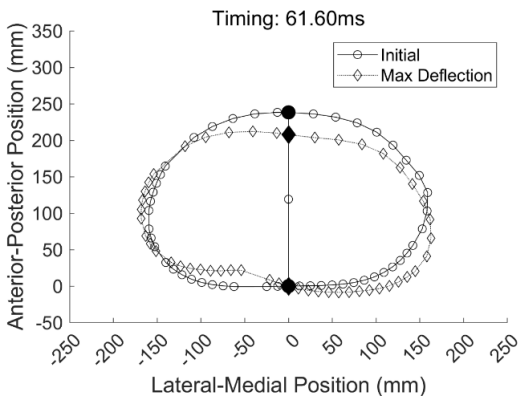

(b) PMHS B (30.7mm, 25.8%)

Fig. 4. Maximum chest A-P deflection

	P	L	A	A	L	P	
R1			N/A	N/A			L1
R2			N/A*	N/A			L2
R3	64.65		65.20*		67.60	64.10	L3
R4	64.60	N/A	61.55		N/A	64.60	L4
R5	65.10		62.15		65.90	65.35	L5
R6			62.30	66.90		65.90	L6
R7			63.65	64.80		N/A	L7
R8			64.85	65.75			L8
R9			68.30	68.45			L9
R10			N/A	68.80			L10
R11			N/A				L11
R12							L12

(a) PMHS A

	P	L	A	A	L	P	
R1	N/A					N/A	L1
R2	N/A				N/A	N/A	L2
R3	62.55		55.30	63.95		57.25	L3
R4	66.30		51.30		61.65	52.50	L4
R5	69.20		60.10			64.05*	L5
R6			60.80	72.35		60.80*	L6
R7			64.25			63.60	L7
R8			64.95				L8
R9			68.30				L9
R10				N/A			L10
R11				N/A			L11
R12							L12

(b) PMHS B

Fig. 5. Rib fracture timing identified from strain gauges at different locations (A= anterior, L=lateral, P=posterior). Green: no fractures, yellow: fracture, * two fractures

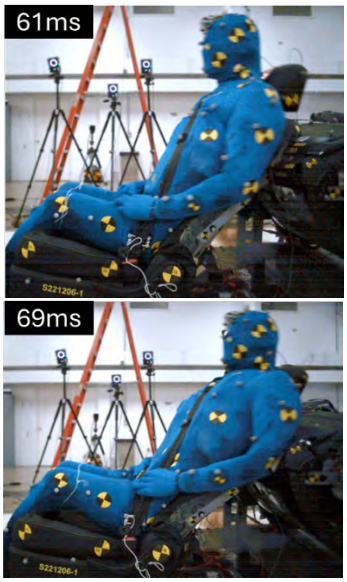

(a) PMHS A

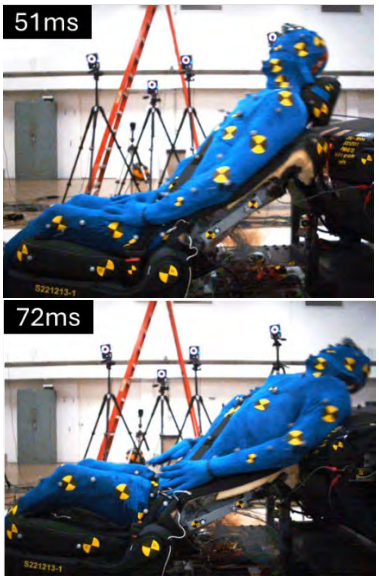

(b) PMHS B

Fig. 6. PMHS kinematics when PMHS were sustaining rib fractures (start and end times)

PMHS Pelvis Kinematics and Strains

Pelvis kinematics transformed from the 6DOF motion blocks installed on the right iliac wing are provided in Fig. 7. Pelvis linear x- and z-accelerations were considerably smaller than those from the ABTS conditions, except for z-acceleration for PMHS A, which was comparable to ABTS25 (Fig. 7a). For Y-rotation, PMHS A pelvis exhibited large rearward rotations as compared to that measured in ABTS25, while the Y-rotation for PMHS B pelvis was consistent with ABTS45 (Fig. 7b). Pelvis angular velocities about x-, y-, and z-axes measured from left and right iliac wings are provided in Fig. C11. It should be noted that angular velocities transformed from both left and right 6DX blocks to the pelvis coordinate system were consistent. The peak y-angular velocities for PMHS A showed an opposite polarity (rearward) compared to the ABTS25 (forward). No clear trends were observed in off-axis angular velocities about x- and z-axes (Fig. C12). Time histories for pelvis kinematics are also provided in Figs. C12-C14.

Strains measured at the left and right superior pubic rami are shown in Fig. C15. Interestingly, a compressive strain mode was observed at both left and right superior pubic rami. For PMHS A, strain measured from the left side (-7389μs) was greater than the right side (-4126μs), while PMHS B exhibited the opposite trend (-5448μs for the left side and -6391μs for right side).

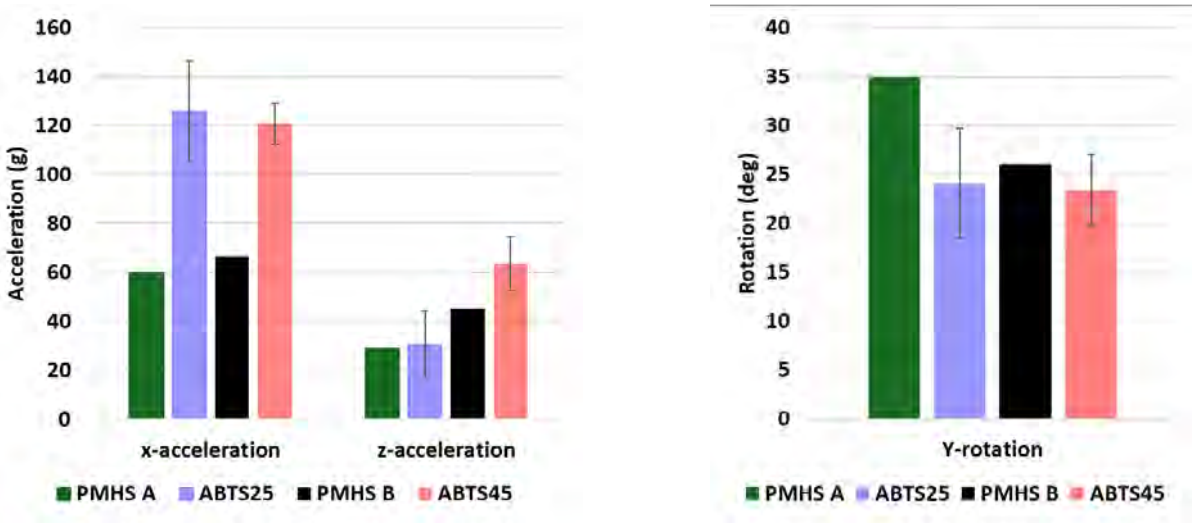

(a) Linear acceleration (b) Y-rotation

Fig. 7. Pelvis kinematics

IV. DISCUSSION

This study explored PMHS whole-body responses and injuries in an unreinforced OEM seat tested in the HSRFFI scenario. Identical sled input to the previous rear-facing PMHS study [5-6] and PMHS instrumentation with additional strain gauge and rosette were utilised in this study. The OEM seat was equipped with an integrated seatbelt with a pretensioner, and PMHS were tested in upright and relaxed recline conditions. An instrumented panel was placed behind the seatback to mimic realistic boundary conditions and avoid seatback collapse during the main event. To better understand the role of a yielding and rotating seatback on PMHS injury outcomes in HSRFFI, the results from the current study were compared to those from previous rear-facing studies [5-6] that used reinforced OEM seats. Regardless of seatback angle (upright vs. relaxed), both PMHS sustained serious (AIS3) to maximal (AIS6) cervical spine injuries likely due to excessive ramping-up motion and hyperextension of the neck (Figs. C2 and C3), critical (AIS5) thoracic injuries likely due to thoracic deformation in the I-S direction, and serious (AIS3) to critical (AIS5) thoracic spine injuries likely due to large angular kinematics at the upper thoracic spine induced from the rotating seatback. Essential instrumentation techniques used in the current study were able to capture hyperextension of the neck, rib principal strain magnitudes and directions, and thoracic spine kinematics and therefore provide confidence in identified injury mechanisms.

Even with the use of unreinforced yielding and rotating seatback conditions, which in theory mitigate energy on the thorax as compared to reinforced conditions, rib fractures still occurred in both PMHS. PMHS A and B each also sustained a pneumothorax (AIS5) and bilateral flail chest (AIS5). It should be noted that none of the PMHS tested in ABTS conditions (ABTS25 and ABTS45) sustained bilateral flail chest [5]. When considering injury outcomes from the FDR condition, for the upright conditions, none of the PMHS tested in FDR25 sustained bilateral flail chest, but one out of four PMHS sustained a pneumothorax in FDR25 [6]. For FDR45, two out of four PMHS sustained bilateral flail chest, and one PMHS sustained pneumothorax in addition to a bilateral flail chest [6]. Recline seatback conditions generally made PMHS rib fractures worse than upright seatback conditions [7]. Having a rotational and yielding seatback did not help to mitigate rib fractures. Upward or I-S thoracic deformation has been discussed as a potential rib fracture mechanism in the HSRFFI [7]. Based on the I-S deformation injury mechanism, PMHS tested in relaxed seatback conditions experienced larger I-S deformation and sustained a high number of rib fractures since the torso orientation became more horizontal (aligned with the sled moving direction) [7]. It should be noted that torso orientation in the unreinforced (rotational and yielding) seatback conditions dynamically rotated rearward and became more horizontal. This dynamic rotation increased the angular momentum of the thorax and negatively affected thoracic I-S deformation and rib fracture outcomes. Maximum chest A-P deflections were 25.7mm for PMHS A and 30.7mm for PMHS B, which were within mean ± one standard deviation (38.9 ± 16.9mm for ABTS25 and 23.7 ± 9.4mm from ABTS45) of the chest A-P

deflections determined in the previous study [7]. Even with comparable maximum chest A-P deflections obtained in this study, the NRF from PMHS tested in the current study were considerably higher than those from the previous study [7]. It should also be noted that the shoulder belt tensions were 537.7N at 61.55ms for PMHS A and 341.5N at 51.30ms for PMHS B when the first anterior rib fractures occurred. These shoulder belt tensions were lower than those measured from relaxed male volunteers (non-injurious) tested in a simulated frontal impact at ΔV of 10kph [15]. Such low chest A-P deflections and shoulder belt tensions cannot explain the rib fracture outcomes in this study. Therefore, these results support the suggestion from [7] that I-S thoracic deformation could be a potential rib fracture mechanism in the HSRFFI.

Strain rosettes were attached to the posterior 6th and 7th ribs to better understand the complicated rib fracture mechanisms. This essential instrumentation allowed for measuring principal strain magnitudes and directions during the events. The maximum principal strain directions of the PMHS tested in the current study, particularly in PMHS A, further support the injury mechanisms of the combined loading of the thorax (A-P and I-S deflections) proposed by [7]. For PMHS B, even with smaller strain magnitudes on the right 6th and 7th ribs, rib fractures occurred around 60 to 64ms, meaning the oblique maximum strain direction, i.e., rib shear and I-S chest deformation, influenced the rib fracture outcomes. PMHS B was tested in the relaxed condition, so the rib angles were more horizontal than in the upright condition, which may affect the maximum principal strain directions. However, further investigation is required to confirm the effect of the rib angle on the principal strain and direction in the relaxed condition, perhaps using HBMs.

Interestingly, both PMHS sustained 1st and 2nd rib fractures on the right and left sides, likely due to interaction with the shoulder belt from excessive ramping-up motion, especially on the right side since the shoulder belt outlet was located at the upper right side of the seatback. It should also be noted that both PMHS A and PMHS B sustained a right distal clavicle fracture. For PMHS B, the uniaxial strain gage installed on the right clavicle indicated fracture occurred at 68.25ms while the PMHS was ramping up, shown in Fig. C16.

Besides this, due to cervical hyperextension, it is also possible that the sternocleidomastoid (SCM) muscles pulled the clavicle and manubrium superiorly, which could deform the upper ribs in the I-S direction. In addition to the SCM muscles, the scalene muscles (anterior, middle, and posterior) could also have influenced I-S deformations due to their direct attachments to the 1st and 2nd ribs. Future work should be performed to understand possible influence of the SCM and scalene muscles on superior rib fractures.

In addition to rib fractures, both PMHS sustained severe cervical and thoracic spine injuries. For the cervical spine injuries, PMHS A and B head x-accelerations were smaller than the ABTS corridors (Figs. 3a and C4a). At the same time, angular kinematics were considerably greater than the ABTS corridors (Figs. 3c, 3e, C4e, and C4g). This means that the current study's unreinforced seatback condition with seatback rotations successfully reduced the linear x-acceleration but increased angular kinematics substantially. The increased angular kinematics resulted in severe cervical spine injuries that have not been observed in previous rear-facing studies [5-7]. Head global rotations about the Y-axis from the current study were greater than 84 degrees regardless of PMHS, which were much larger than the ABTS PMHS head rotations, likely due to the large seatback rotations (Figs. C2 and C3). Based on the results from this study, head angular kinematics should be minimised to avoid possible cervical spine injuries by reducing seatback rotation and minimising ramping-up motion. Once the seatback starts rotating, PMHS linear momentum becomes smaller, but as a trade-off, angular momentum increases, which results in increased tangential velocity of the PMHS. After tangential velocity increases, centripetal or radial acceleration increases, influencing ramping-up motion along the seatback. The larger the seatback rotation, the larger the ramping-up motion. Therefore, the risk of cervical hyperextension injuries inevitably increases. The PMHS kinematics when the hyperextension occurred can be seen in Figs. C2 and C3. Based on this, unreinforced seatbacks with large rotations may have adverse effects on cervical spine injury outcomes in HSRFFI conditions. For rear-facing impacts, the seatback may have to be stiffened to protect against cervical spine injury, which makes whiplash protection in low-speed rear impacts difficult. Future research should be conducted to find optimal seatback strength to protect against cervical spine injuries in low-speed rear impacts and HSRFFI conditions, which may require active safety concepts.

In the previous reinforced seat PMHS tests (ABTS [5] and FDR [6]), only one out of 14 PMHS (PMHS3 in ABTS25 [5]) sustained thoracic vertebral body fractures, and it was due to pre-existing spine condition (osteophyte formation between T10 and T11). Surprisingly, both PMHS tested in the current study sustained serious (or worse) thoracic spine injuries (PMHS A: complete spinal cord transection with bilateral dislocation and fracture at T4/T5,

PMHS B: vertebral body fracture at T1) likely due to large rearward rotation of the upper thoracic spine (Figs. 3f, C2, C3, and C5). Peak x-accelerations measured at T1 and T4 in PMHS A and PMHS B were lower than those measured from ABTS25 and ABTS45 conditions (Figs. 3 and C5), yet thoracic spine injuries occurred, suggesting linear x-acceleration may not be an injury predictor. However, peak y-angular velocities measured from PMHS A and B were greater than those seen in ABTS conditions, indicating y-angular velocity may be a better injury predictor. Peak y-angular velocities measured from PMHS A and PMHS B were 4216deg/s and 3599deg/s at T1 (Fig. 3d), 3328deg/s and 1648deg/s at T4 (Fig. C6d), 1409deg/s and 1551deg/s at T8 (Fig. C6e), and 665deg/s and -992deg/s at T12 (Fig. C6f), respectively. For PMHS A, peak y-angular velocities at T1 and T4 (upper thoracic spine) were more than double the y-angular velocity measured at T8 and T12, indicating that the upper thoracic spine in PMHS A experienced large extension angular momentum during the event. As a result, the PMHS sustained critical injury at T4/T5. For PMHS B, the difference in y-angular velocity between T1 and T4 was more than double, which can explain the major vertebral body fracture at T1. It should be noted that the upper thoracic angular velocity is likely to be influenced by upper thoracic spine curvature and spine straightening during the event [5]. These should be investigated further to understand injury mechanisms of the thoracic spine in HSRFFI conditions. Nonetheless, the unreinforced seatback negatively affected thoracic spine injury compared to the reinforced seat conditions (ABTS and FDR).

PMHS tested in the current study did not sustain pelvic fractures, so the unreinforced OEM seat successfully dissipated energy in the pelvic area, which was observed in the pelvis kinematics, primarily linear x-accelerations (Figs. 6 and C12). Nine out of 14 PMHS sustained pelvic fractures in the previously tested reinforced seatback conditions (ABTS and FDR). Three PMHS sustained severe superior and inferior pubic ramus fractures along with sacroiliac joint damage. The previous study proposed open book deformations (outward deformations) of the pelves induced from inertial loading from the lower limb and seatback reaction force as a possible injury mechanism [6]. If a pelvis experienced open book deformation, strains at the superior pubic rami are likely to be tensile. However, the strain mode measured at the superior pubic rami was compressive in the current study, which may be expected due to the pelvis pocketing into the seatback and the rotating seatback. This may be helpful information for design engineers to develop and improve seats when considering rear-facing scenarios. FE HBMs can be used to measure strain at the superior pubic rami when new seats are designed and developed. A design target could be the occurrence of compressive strain or minimising tensile strain at the superior pubic rami to prevent pelvic open book deformation.

As the human body is a kinetic and kinematic chain, energy seemed to be successfully dissipated in the pelvic region using an unreinforced OEM seat as pelvic accelerations in the x-direction measured from PMHS A and PMHS B were considerably lower than those measured from PMHS tested in the reinforced or rigidized OEM seats [5], shown in Figs. C12(a) and C12(b). However, adversely, the linear accelerations increased in the legs. Consequently, both PMHS sustained proximal fibula fractures (PMHS A: only left side, PMHS B: both left and right sides) instead of pelvic fractures that have been found in the previous studies [5-7]. The sequential PMHS motions (Figs. C2 and C3) clearly show leg interactions with the front portion of the seat pan. After 100ms, the legs quickly rotated upwards (extension) due to high loads applied to the legs. Right tibia x-accelerations are provided in Fig. C17. Right tibia x-acceleration showed higher acceleration (100.1g for PMHS A and 130.8g for PMHS B) compared to ABTS25 (87.8 ± 24.4g) and ABTS45 (107.3 ± 17.9g) (Fig. C17), which demonstrates higher loading in the leg region compared to ABTS conditions. The tibia x-accelerations (Fig. C17) were also higher than pelvis x-acceleration (Figs. C12 and C17), indicating higher inertial loading was applied to the tibiae than the pelves. For the previous study, two out of 14 PMHS tested in reinforced seatback conditions (ABTS45 and FDR45) sustained fibula fractures. Regardless of reinforcement conditions, tibia accelerations from the relaxed conditions (PMHS B and ABTS45) were greater than the upright conditions (PMHS A and ABTS25) shown in Fig. C17, implying that a reclined seatback may increase the risk of lower extremity injury in HSRFFI conditions.

Limitations

A small sample size is one of the main limitations of this study. Only two PMHS were tested to explore the effect of unreinforced seatback on PMHS injury risks. However, rib strain, principal strain and direction, chest A-P deformation, and pelvis strain data are sparse in the literature. This study provides valuable information that can help understand injury mechanisms for the unreinforced seat in the HSRFFI condition.

PMHS age could have affected the injury severities in this study. PMHS A and PMHS B were older than the average age of the PMHS tested in [5-6], although their aBMD t-scores were higher (+2.7 for PMHS A and +1.7 for PMHS B) than the average aBMD (0.2 ± 1.3) of the PMHS tested in [5-6].

Only one seat was used in this study. Different foam types and properties in different seats may result in different injury outcomes. Once HBMs are enhanced, seatback strength, stiffness, and properties can be optimised using multiple FE HBM simulations.

A single gap (100mm) between the back of the seatback and front of the IP was used in this study. Gap size was chosen to ensure enough space for new seatback airbag designs, which will be tested in future PMHS tests. The gap was set to be the same (100mm) between the upright and relaxed conditions to control testing variables and ensure consistency between the conditions. However, the 100mm distance used in the relaxed seatback condition may not be realistic due to the limited adjustability and availability of seat space in vehicles. The feasibility and sensitivity of using different gaps on the PMHS responses and injuries should be explored in future studies.

A single OEM seat with an integrated seatbelt and pretensioner was used in this study. Characteristics of the OEM seatback frame, structure, and foam were not designed for the high-speed rear-facing frontal impact conditions, but low-speed rear impacts may have been considered in the design. Therefore, the PMHS responses and injuries documented in this study are only valid in the OEM seat at high-speed rear-facing frontal impact conditions employed in the current study. Different seatback characteristics could result in different injury types, patterns, and locations. Although the OEM seat might exaggerate PMHS ramping-up motions and relevant injury outcomes, it is still important to explore PMHS biomechanical responses and injuries in worst-case scenarios since current ATDs and HBMs should be enhanced against a various range of PMHS testing data.

Although previously published ABTS responses and corridors were compared to results from the current study, the OEM seat used in the current study was not the same model and manufacture as the ABTS OEM seat. Therefore, comparison and interpretation of the data should be made with caution. However, due to limited biomechanical data and corresponding injury outcomes from unreinforced HSRFFI conditions, the information presented in this study should provide useful insights for designing safer seats to mitigate injuries.

V. CONCLUSION

It has been argued that a reinforced seat contributed to severe injuries, such as rib and pelvis fractures in previous studies. This study investigated male PMHS responses and injuries using an unreinforced OEM seat in rear-facing frontal impacts. PMHS still sustained a critical number and distribution of rib fractures, i.e., bilateral flail chest, in the unreinforced rear-facing seat configurations, regardless of the recline angle. The rib fractures were likely due to the A-P chest compression with the large I-S thorax deflection induced by the ramping motion and seatback rotation, which was supported by strain rosette results. The yielding seatback considerably increased rearward head angular kinematics, which resulted in serious (or worse) cervical and thoracic spine injuries regardless of recline angles. Pelvis fractures were not observed; however, fibula fractures were sustained, which suggests more energy was transferred to the lower extremity when the seatback deformed and rotated rearward. PMHS tested in unreinforced seat configurations in high-speed rear-facing impacts were lacking in literature. The results from this study provide information that can be used as a guideline for designing rear-facing seats in vehicles with automated driving systems and can be utilised to make HBM improvements in new crash conditions.

VI. ACKNOWLEDGEMENTS

We would like to acknowledge the anatomical donors of The Ohio State University. Without these selfless gifts, it would be impossible to conduct this research. We would also like to thank Hyundai Mobis for sponsoring this study. The opinions expressed within are solely those of the authors and do not represent the views of any sponsors or collaborators. This study would not have been possible without the tremendous contributions of students, staff, and faculty at the Injury Biomechanics Research Center at The Ohio State University.

VII. REFERENCES

[1] McMurry TL, Poplin GS, Shaw G, Panzer MB. (2018) Crash safety concerns for out of position occupant postures: A look toward safety in highly automated vehicles. *Traffic Injury Prevention*, **19**(6):582-587.
[2] Koppel, S., Jiménez Octavio, J., Bohman, K., Logan, D., et al. (2019) Seating configuration and position preferences in fully automated vehicles. *Traffic Injury Prevention*, **20**(sup2): S103-S109.
[3] Jorlöv, S., Bohman, K., Larsson, A., (2017) Seating positions and activities in highly automated cars–a qualitative study of future automated driving scenarios. *Proceedings of International Conference on the Biomechanics of Impact (IRCOBI)*, 2017, IRC-17-11. Antwerp, Belgium.
[4] Östling, M., Larsson, A. (2019) Occupant activities and sitting positions in automated vehicles in China and Sweden. *Proceedings of 26th International Technical Conference on the Enhanced Safety of Vehicles (ESV)*, 2019, pp. 10-13. Eindhoven, Netherlands.
[5] Kang Y., Stammen J., Ramachandra R., Agnew A.M., Hagedorn A., Thomas C., Kwon H.J., Moorhouse K., Bolte J.H. (2020) Biomechanical responses and injury assessment of post mortem human subjects in various rear-facing seating configurations. *Stapp Car Crash Journal*, **64**: 155–212.
[6] Kang Y., Stammen J., Bendig A., Agnew A.M., Hagedorn A., Thomas C., Ramachandra R., Kwon H.J., Moorhouse K., Bolte JH. (2022) Effects of seat back recline and belt restraint type on PMHS responses and injuries in rear-facing frontal impacts. *SAE International Journal of Transportation Safety*, **10**(2):235–289.
[7] Kang Y., Stammen J., Agnew A., Baker G., Pradhan V., Bendig A., Hagedorn A., Moorhouse K., Bolte J. (2023) Thoracic responses and injuries to male postmortem human subjects (PMHS) in rear facing seat configurations in high-speed frontal impacts. *Traffic Injury Prevention*, **24**(sup1): S47-S54.
[8] Linder A, Avery M, Krafft M, Kullgren A. (2003) Change of velocity and pulse characteristics in rear impacts - real world and vehicle tests data. *Proceedings of 18th International Technical Conference on the Enhanced Safety of Vehicles*, Nagoya, Japan. Paper No. 285
[9] Viano DC, Parenteau CS. (2008) Serious injury in very-low and very-high speed rear impacts. *SAE Technical Paper* 2008-01-1485.
[10] Zellmer H, Lubbe N, Sander U. (2018) Assessing the Injury Risk of Car Occupants on Rearward Facing Seats–An Analysis of GIDAS Cases. *Proceedings of 8th ESAR Conference*. Hannover, Germany.
[11] Ngo AV, Becker J, Thirunavukkarasu D, Urban P, Koetniyom S, Carmai J. (2021) Investigation of occupant kinematics and injury risk in a reclined and rearward-facing seat under various frontal crash velocities. *Journal of Safety Research*, **79**, 26-37.
[12] SAE (2007) Instrumentation for Impact Test - Part 1 Electronic instrumentation. *Society of Automotive Engineers,* Paper No. J211/1_202208.
[13] Reed MP, Ebert SM, and Jones ML. (2019) Posture and belt fit in reclined passenger seats. *Traffic Injury Prevention*, **20**(sup1):S38-S42.
[14] AIS (2015), Abbreviated Injury Scale—2015 Revision, AAAM, Des Plaines, IL.
[15] Kemper AR, Beeman SM, Madigan ML, Duma, SM. (2014). Human occupants in low-speed frontal sled tests: effects of pre-impact bracing on chest compression, reaction forces, and subject acceleration. *Traffic Injury Prevention*, **15**(sup1): S141-S150.

VIII. APPENDIX

Appendix A

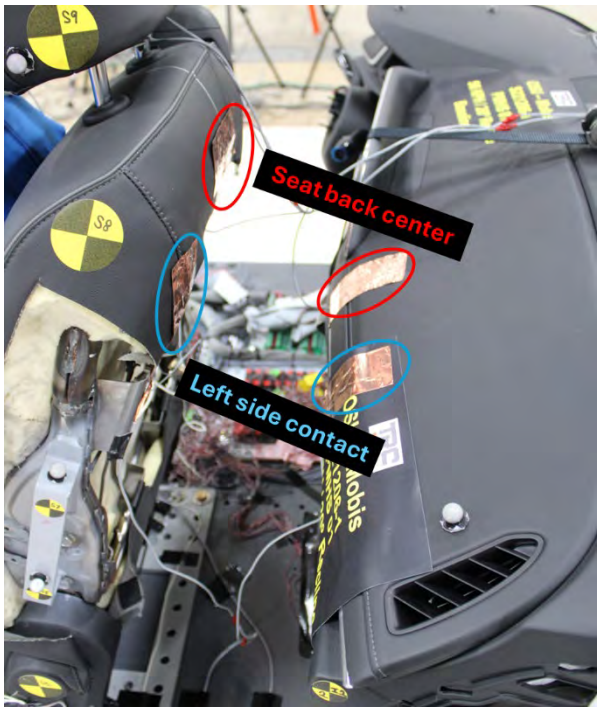

Fig. A1. Contact switches using conductive tape to record seatback-to-IP contact timing

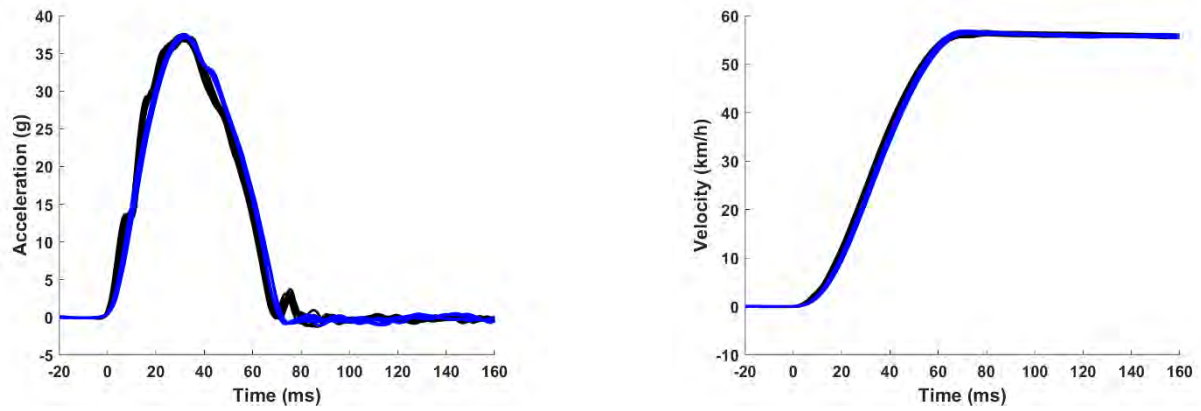

(a) Sled acceleration (b) Sled velocity

Fig. A2. Sled pulse (blue: current study, black: previous study [7]). Coefficients of variation (CV) using peak values were less than 2%

Appendix B

TABLE BI
ANTHROPOMETRY MEASUREMENTS (CM)

	PMHS A	PMHS B	ABTS PMHS Mean (SD) [5]
VRTSYM	84.7	88.3	87.8 (2.9)
HEADCH	22.0	19.0	21.2 (1.9)
HEADLN	19.1	17.9	18.9 (0.4)
HEADBD	15.5	13.9	14.3 (0.7)
HEADCR	57.8	55.5	57.9 (1.6)
NECKBD	11.8	9.7	10.7 (1.3)
NECKCR	44.4	38.6	40.2 (5.2)
NECKDP	14.6	12.6	12.6 (2.0)
SHLDHT	145.6	142.0	150.2 (5.5)
SHLDBD	39.6	36.7	37.9 (3.0)
INSCYE	57.5	51.5	47.5 (6.1)
CHSTBD	35.8	33.4	33.1 (3.4)
CHSTCR	107.5	94.6	98.5 (8.0)
CHSTDP	23.6	21.0	20.6 (1.8)
WASTBD	33.0	30.2	31.0 (1.7)
WASTCR	101.8	87.6	95.5 (9.5)
WASTDP	23.0	18.2	20.3 (3.0)
HIPBD	34.7	31.7	33.3 (1.3)
HIPCR	102.5	89.0	97.4 (5.5)
TRCPAT	41.4	41.5	40.6 (2.0)

VRTSYM: vertex to symphysion length
HEADCH: vertex-mentum
HEADLN: max between glabella and occiput
HEADBD: head breadth
HEADCR: head circumference
NECKBD: neck breadth
NECKCR: neck circumference
NECKDP: neck depth at laryngeal prominence
SHLDHT: shoulder height
SHLDBD: shoulder breadth
INSCYE: interscye distance
CHSTBD: chest breadth
CHSTCR: chest circumference
CHSTDP: chest depth
WASTBD: waist breadth
WASTCR: waist circumference
WASTDP: waist depth
HIPBD: hip breadth
HIPCR: hip circumference
TRCPAT: trochanter to patella distance

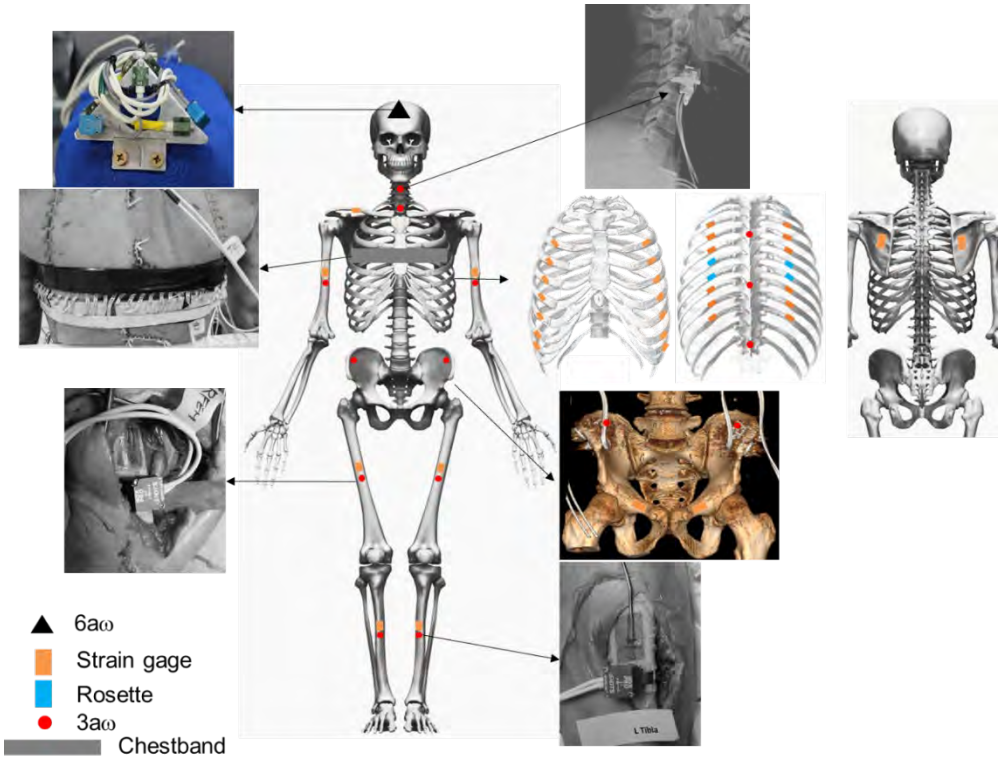

Fig. B1. PMHS instrumentation overview

TABLE BII
PMHS SEATING POSTURE
MEASURED VALUE
(TARGET VALUE ± ALLOWABLE RANGE)

	PMHS A	PMHS B
Head angle (deg)	0.8 (0.0 ± 2.0)	24.3* (19.7 ± 2.0)
Hip to eye angle (deg)	89.7 (81.6 ± 5.0)	65.1 (63.4 ± 5.0)
Backset (mm): head-to-head restraint distance	83.0 (N/A)	0.0 (N/A)
*Pelvis angle** (deg): greater trochanter to L5S1*	36.0 (40.1 ± 5.0)	23.5 (27.3 ± 5.0)
Thigh angle (deg)	12.2 (12.9 ± 2.0)	10.5 (11.8 ± 2.0)
Leg angle (deg)	45.7 (44.3 ± 2.0)	45.3 (44.7 ± 2.0)

* could not achieve target range
** pelvis angle was determined using X-ray image

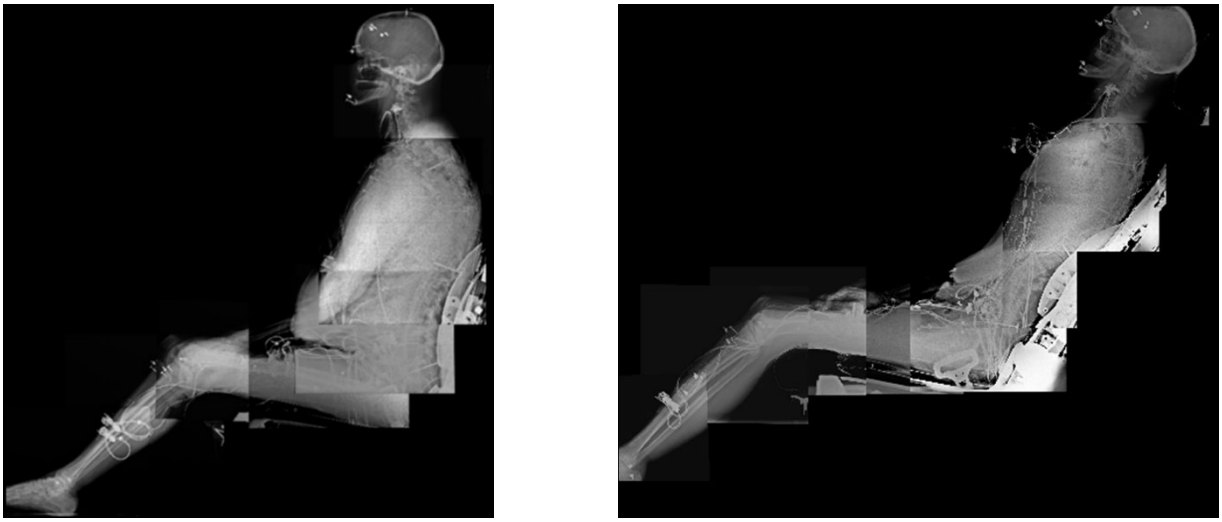

(a) PMHS A (b) PMHS B

Fig. B2. Stitched X-ray images of PMHS.. seated in test positions

(a) PMHS A (b) PMHS B

Fig. B3. 3D FARO scan of PMHS seated in test positions

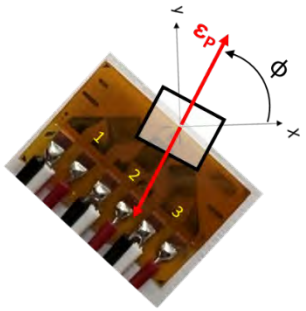

Fig. B4. Strain rosette (45deg array) coordinate system. Ɛp: principal strain and Φ: principal strain angle

Appendix C

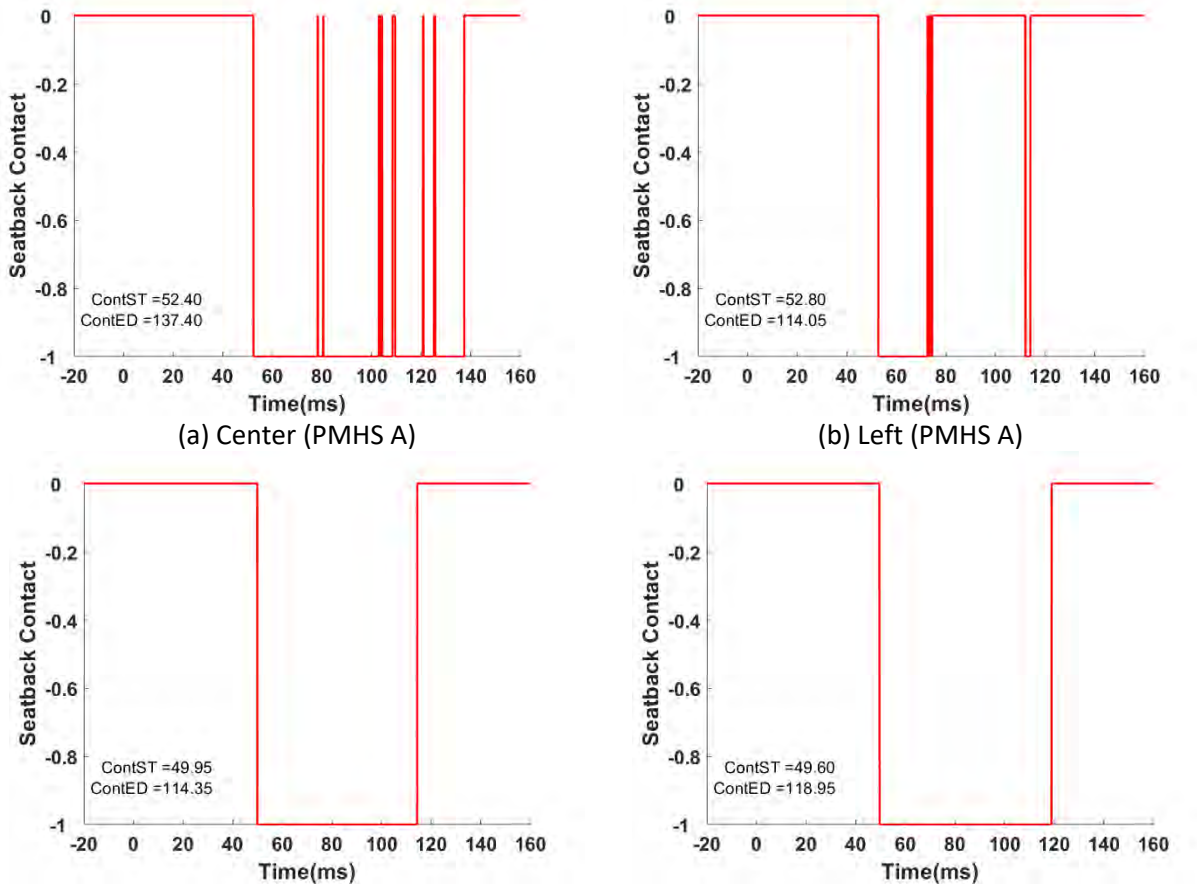

(a) Center (PMHS A) (b) Left (PMHS A)

(c) Center (PMHS B) (d) Left (PMHS B)

Fig. C1. Seatback-to-IP contact timing. ConST: contact start time, ConED: contact end time

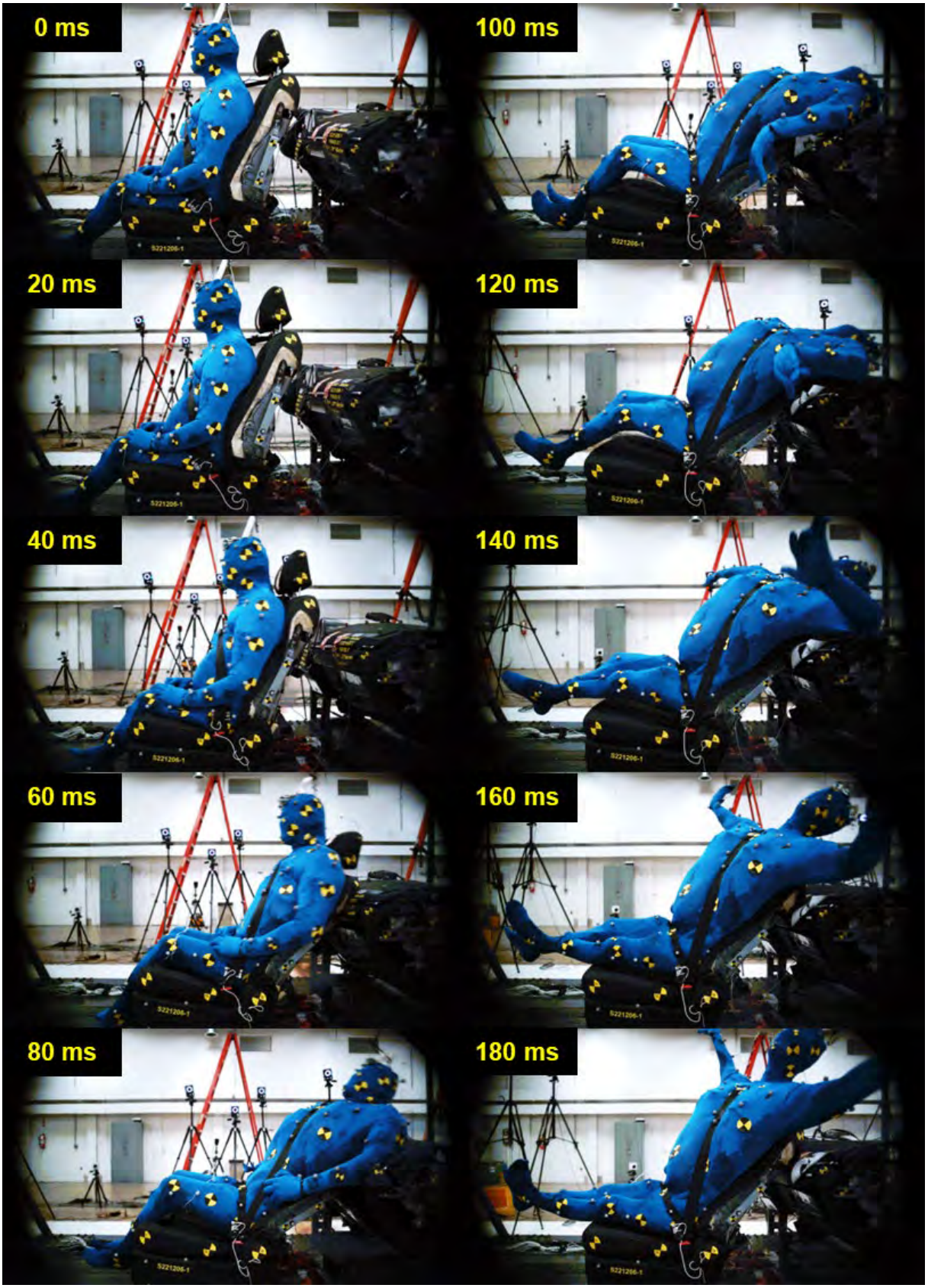

Fig. C2. Sequential whole-body motions from a side-view high-speed video (PMHS A)

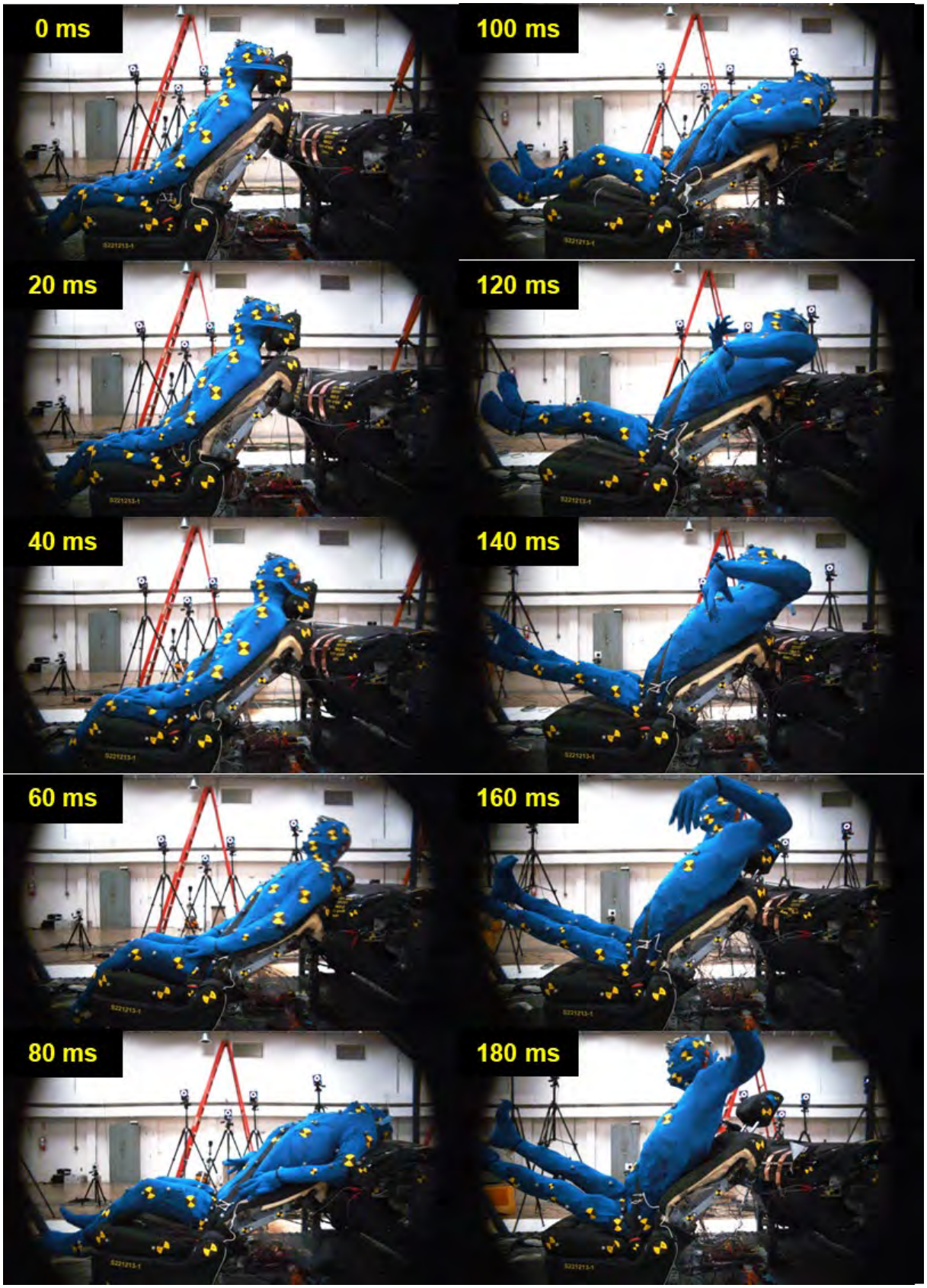

Fig. C3. Sequential whole-body motions from a side-view high-speed video (PMHS B)

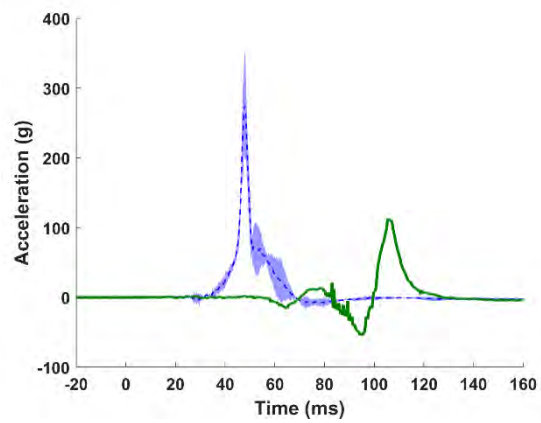

(a) Acceleration in x-direction (PMHS A)

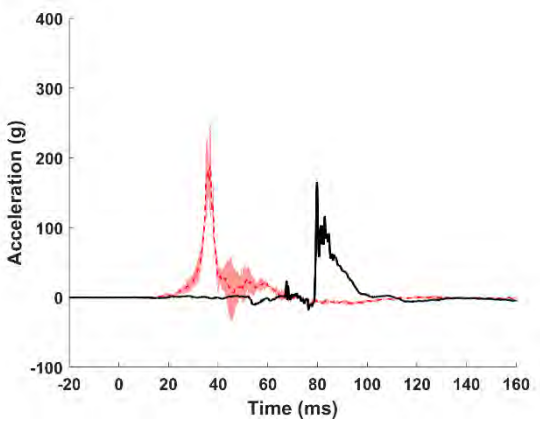

(b) Acceleration in x-direction (PMHS B)

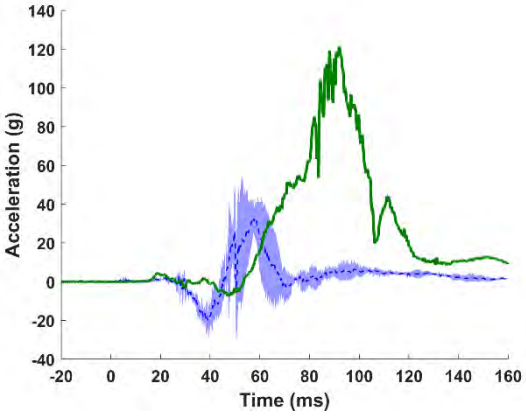

(c) Acceleration in z-direction (PMHS A)

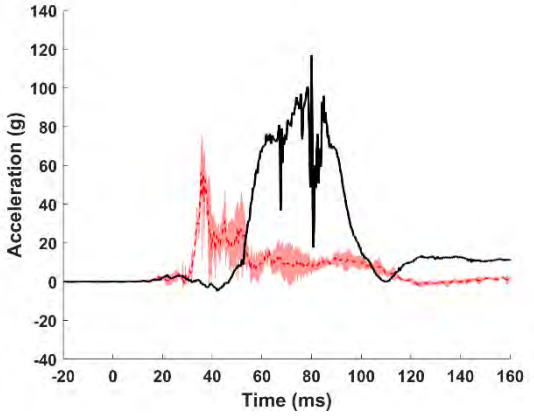

(d) Acceleration in z-direction (PMHS B)

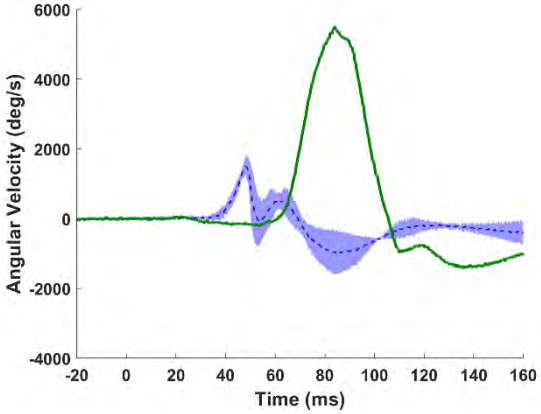

(e) Angular velocity about y-axis (PMHS A)

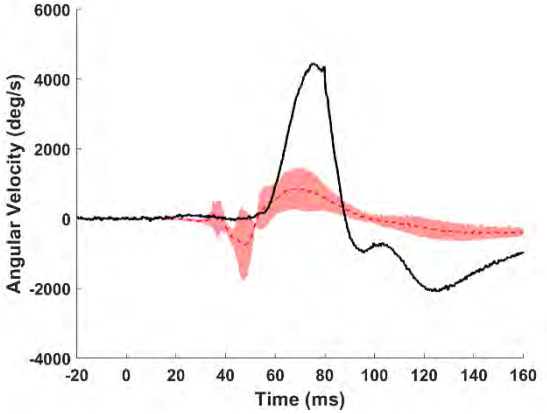

(f) Angular velocity about y-axis (PMHS B)

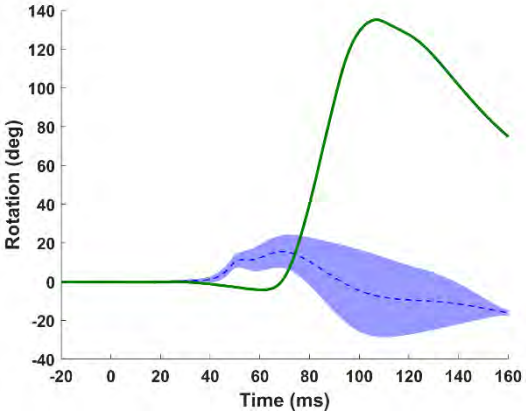

(g) Rotation about Y-axis (PMHS A)

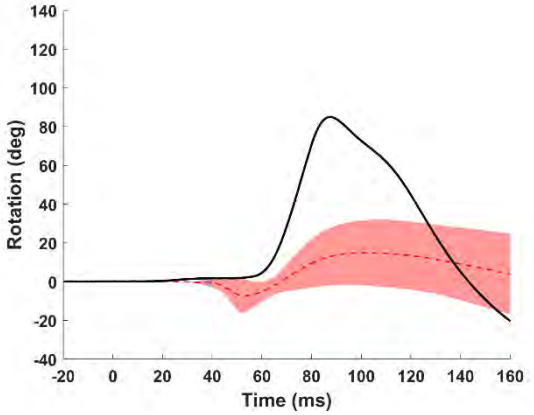

(h) Rotation about Y-axis (PMHS B)

Fig. C4. Head kinematics. Blue corridor: ABTS25 (N=3 [5]), red corridor: ABTS45 (N=3 [5]), green curve: PMHS A, black curve: PMHS B

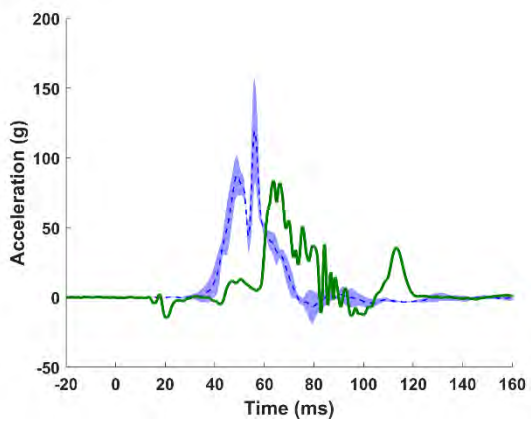

(a) Acceleration in x-direction (PMHS A)

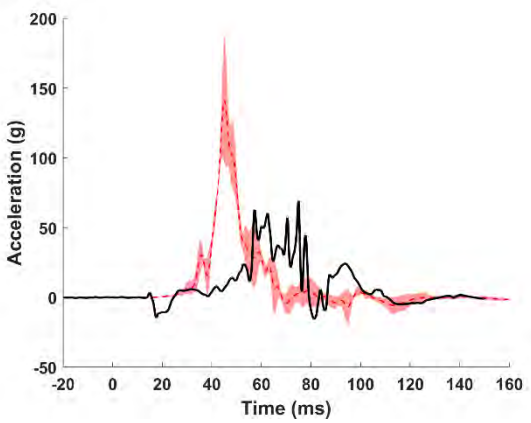

(b) Acceleration in x-direction (PMHS B)

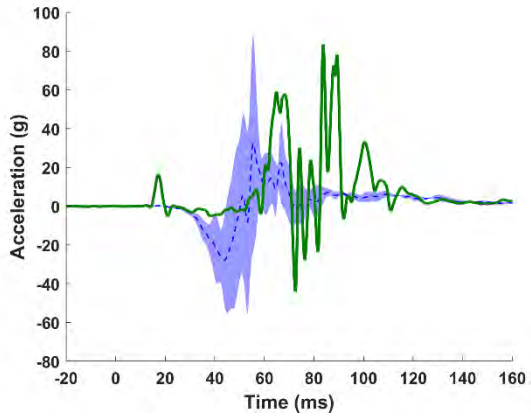

(c) Acceleration in z-direction (PMHS A)

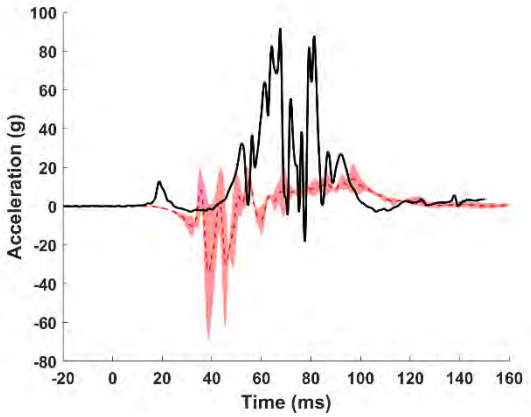

(d) Acceleration in z-direction (PMHS B)

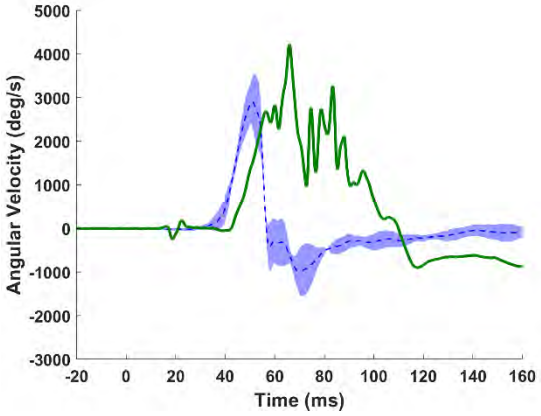

(e) Angular velocity about y-axis (PMHS A)

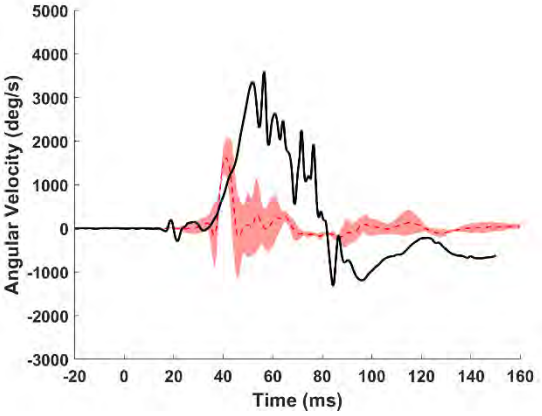

(f) Angular velocity about y-axis (PMHS B)

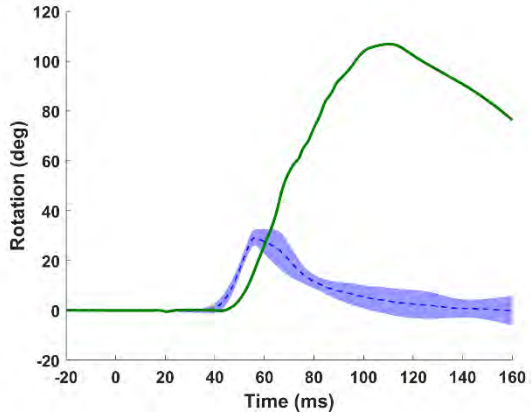

(g) Rotation about Y-axis (PMHS A)

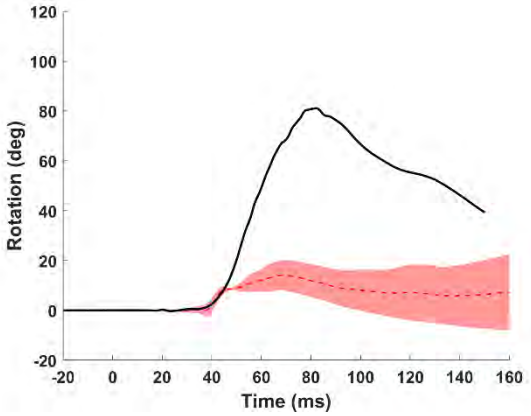

(h) Rotation about Y-axis (PMHS B)

Fig. C5. T1 kinematics. Blue corridor: ABTS25 (N=3 [5]), red corridor: ABTS45 (N=3 [5]), green curve: PMHS A, black curve: PMHS B

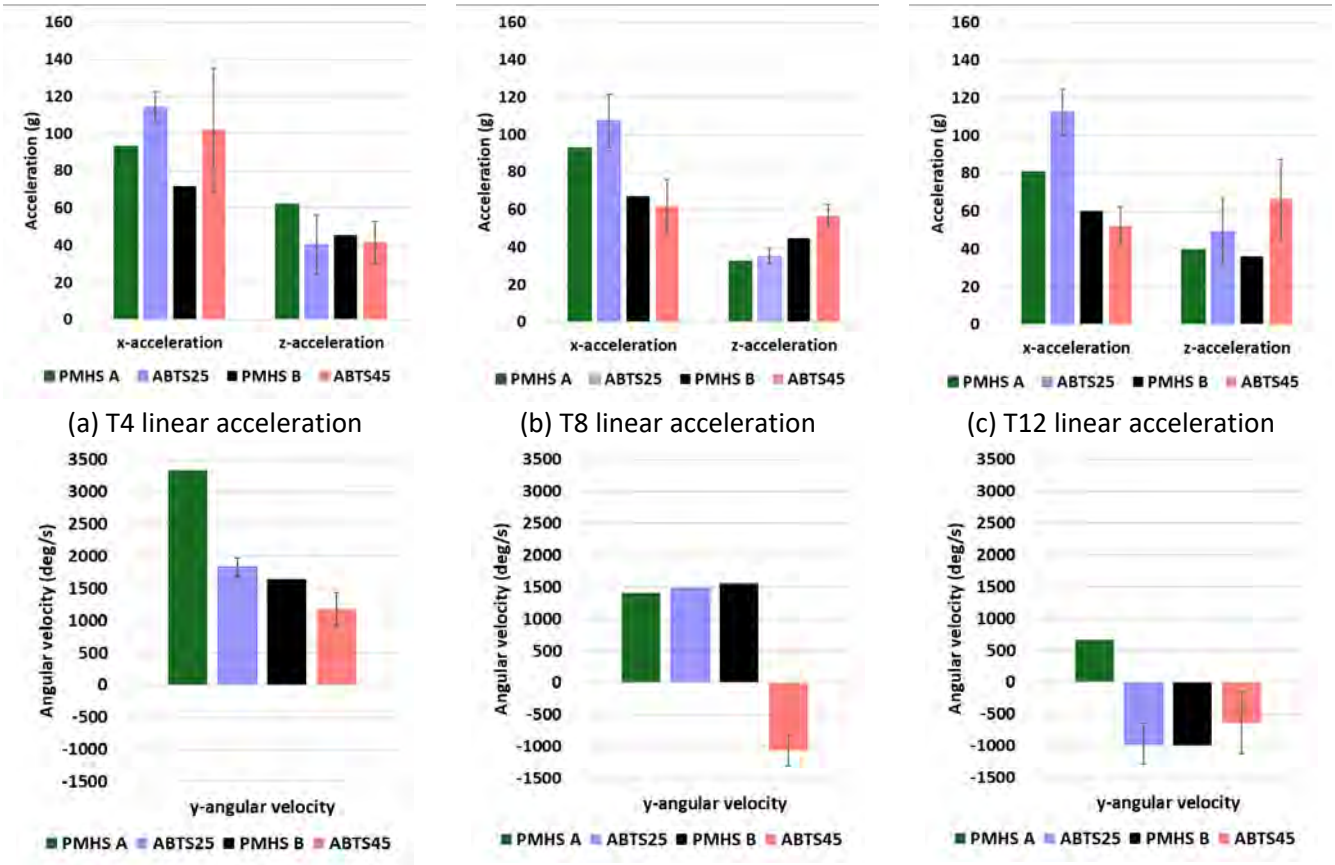

(a) T4 linear acceleration (b) T8 linear acceleration (c) T12 linear acceleration

(d) T4 angular velocity about y-axis (e) T8 angular velocity about y-axis (f) T12 angular velocity about y-axis

Fig. C6. Peak values from T4, T8, and T12 kinematics

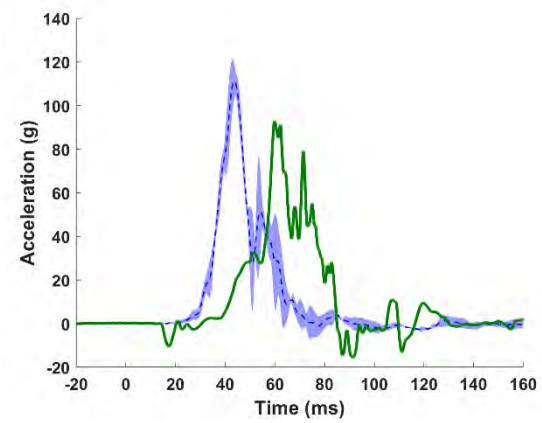

(a) Acceleration in x-direction (PMHS A)

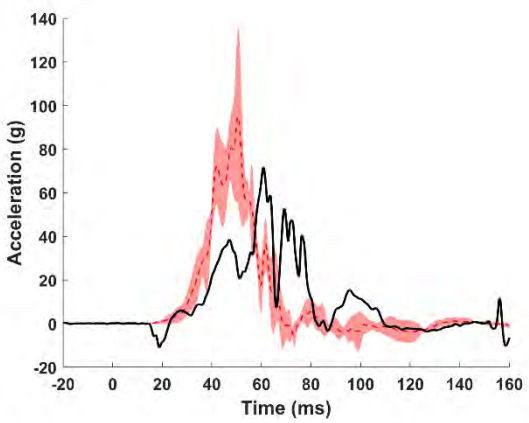

(b) Acceleration in x-direction (PMHS B)

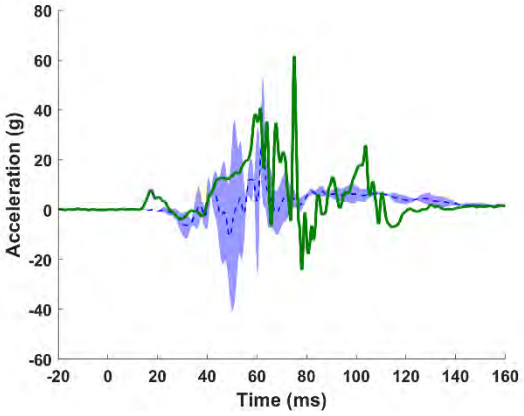

(c) Acceleration in z-direction (PMHS A)

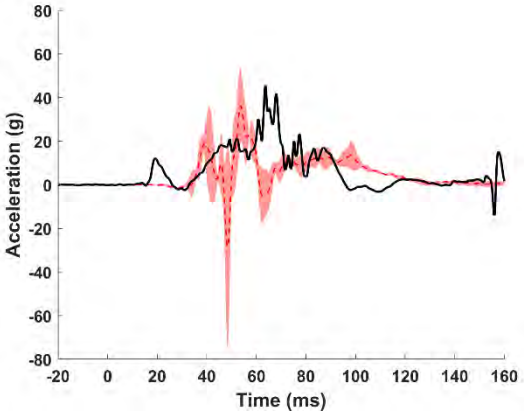

(d) Acceleration in z-direction (PMHS B)

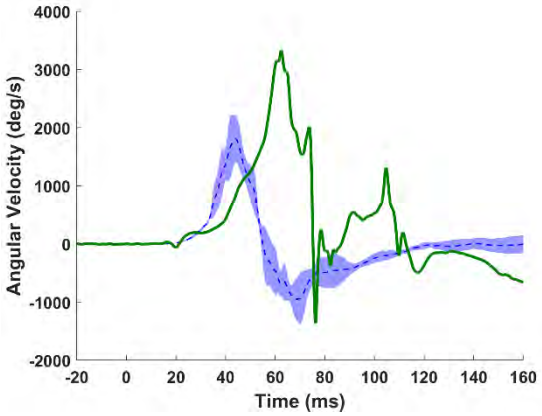

(e) Angular velocity about y-axis (PMHS A)

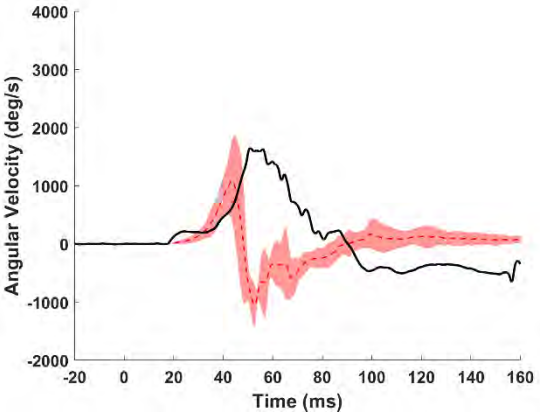

(f) Angular velocity about y-axis (PMHS B)

Fig. C7. T4 kinematics. Blue corridor: ABTS25 (N=3 [5]), red corridor: ABTS45 (N=3 [5]), green curve: PMHS A, black curve: PMHS B

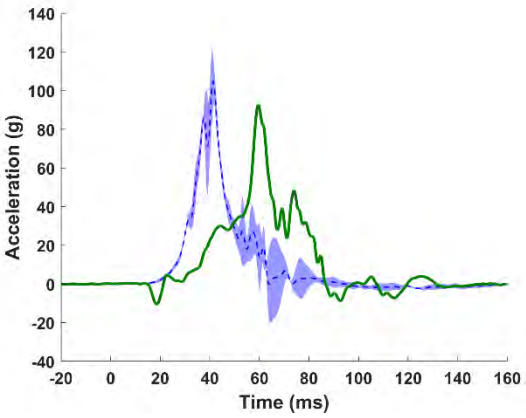

(a) Acceleration in x-direction (PMHS A)

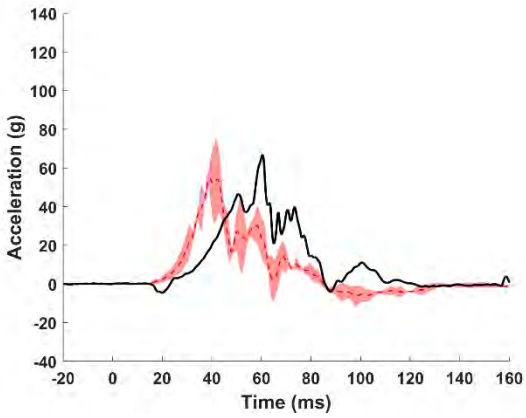

(b) Acceleration in x-direction (PMHS B)

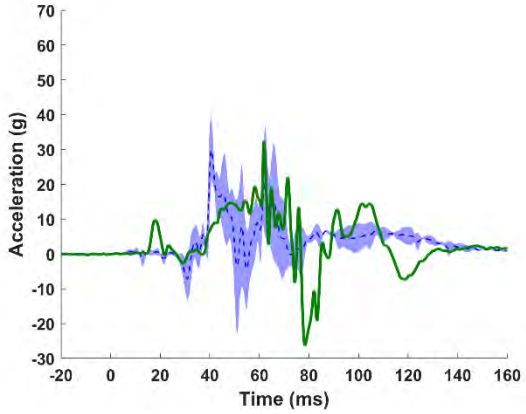

(c) Acceleration in z-direction (PMHS A)

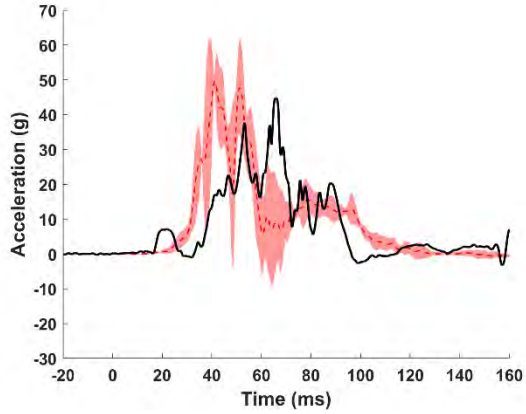

(d) Acceleration in z-direction (PMHS B)

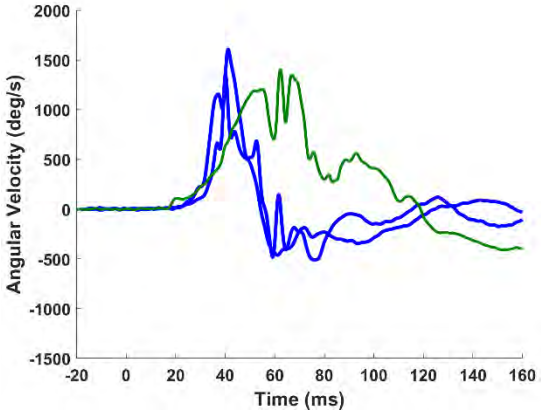

(e) Angular velocity about y-axis (PMHS A)*

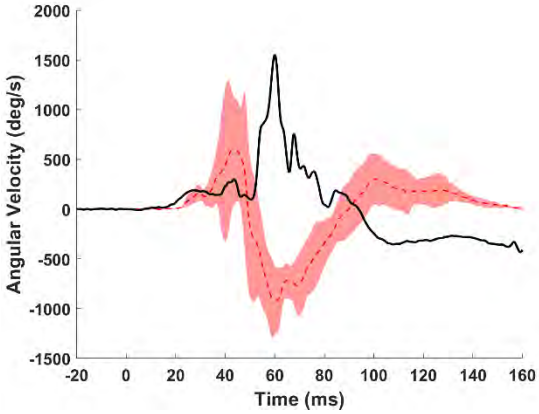

(f) Angular velocity about y-axis (PMHS B)

Fig. C8. T8 kinematics Blue corridor: ABTS25 (N=3 [5]), red corridor: ABTS45 (N=3 [5]), green curve: PMHS A, black curve: PMHS B

* No corridor was available so two individual PMHS curves were plotted.

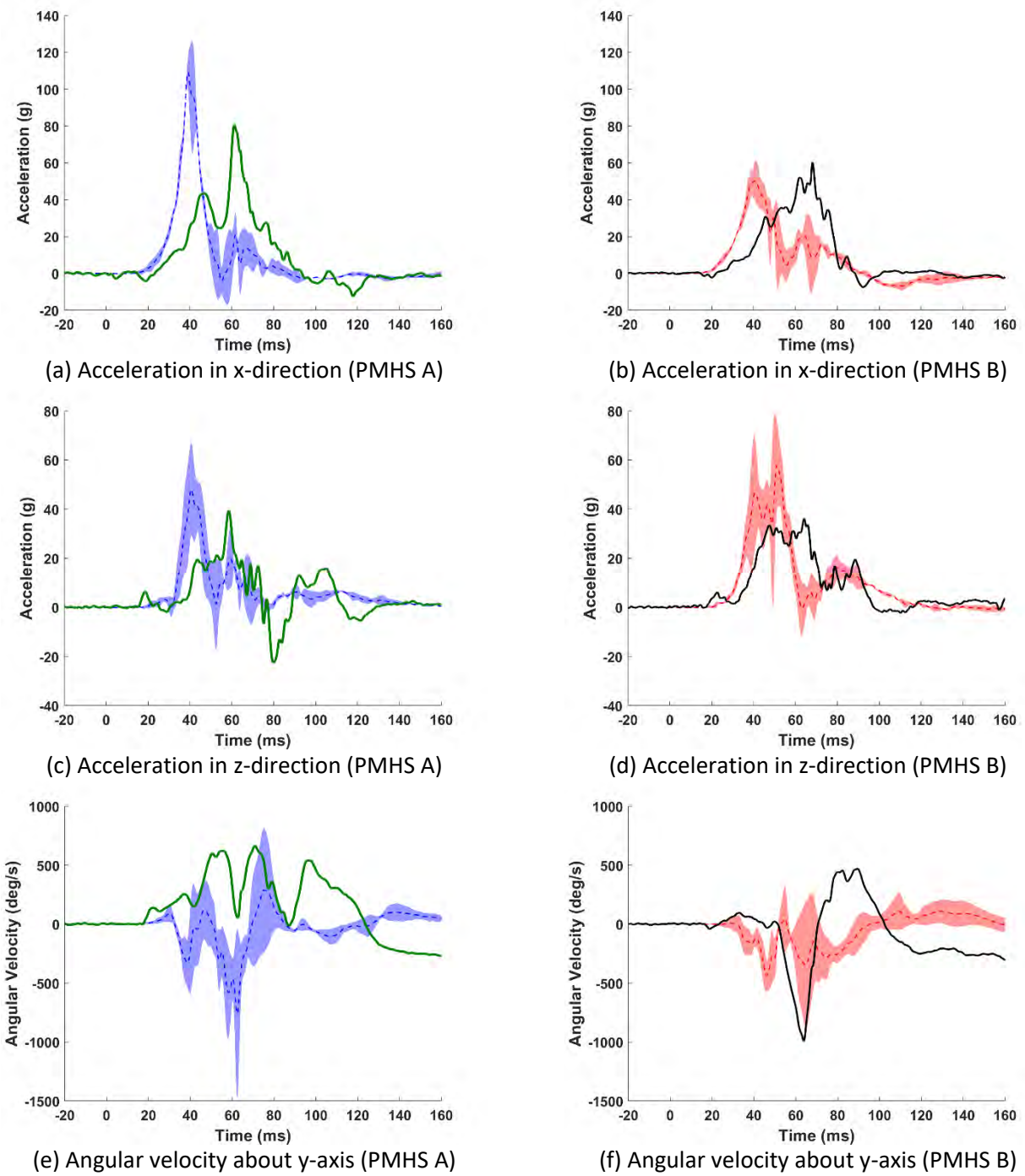

(a) Acceleration in x-direction (PMHS A)

(b) Acceleration in x-direction (PMHS B)

(c) Acceleration in z-direction (PMHS A)

(d) Acceleration in z-direction (PMHS B)

(e) Angular velocity about y-axis (PMHS A)

(f) Angular velocity about y-axis (PMHS B)

Fig. C9. T12 kinematics. Blue corridor: ABTS25 (N=3 [5]), red corridor: ABTS45 (N=3 [5]), green curve: PMHS A, black curve: PMHS B

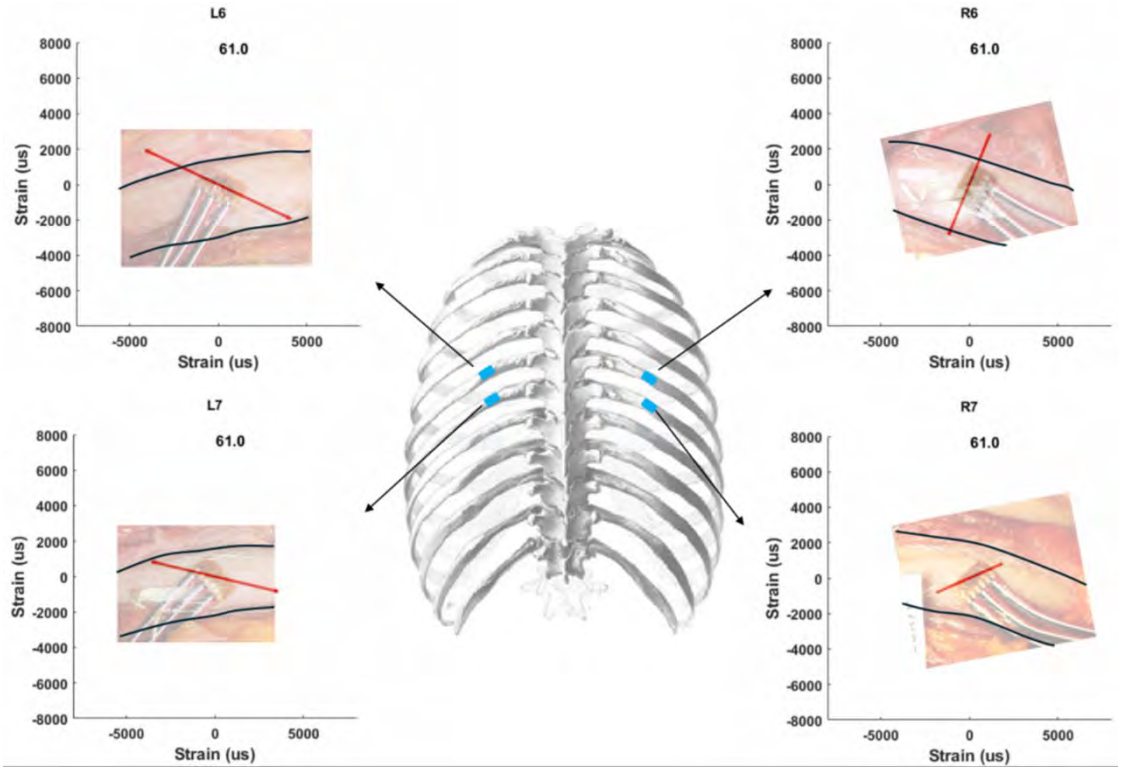

(a) PMHS A

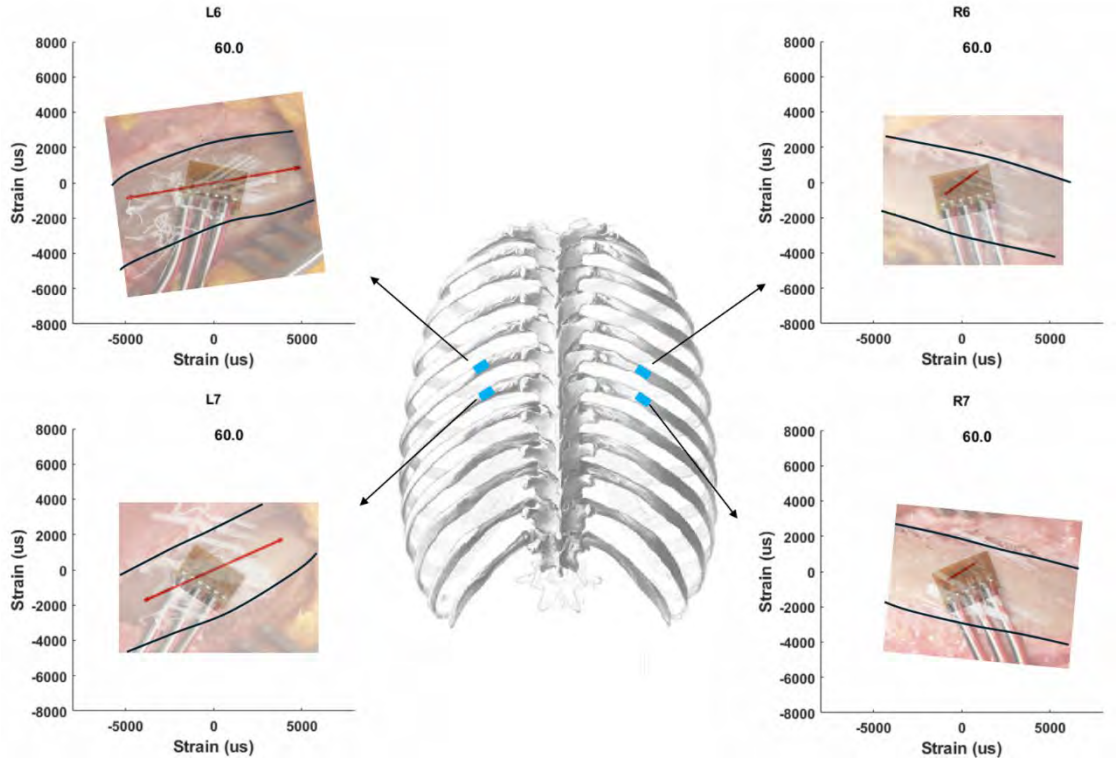

(a) PMHS B

Fig. C10. Maximum principal strain magnitude and angle measured at left and right 6th and 7th ribs (L6, L7, R6, and R7). Pictures embedded in the plots show strain rosettes attached to the ribs. Black lines were added to indicate rib boundaries in the pictures. Red arrow length indicates the principal strain magnitude, while orientations represent the principal strain angle at 60 and 61ms when the first anterior rib fracture occurred.

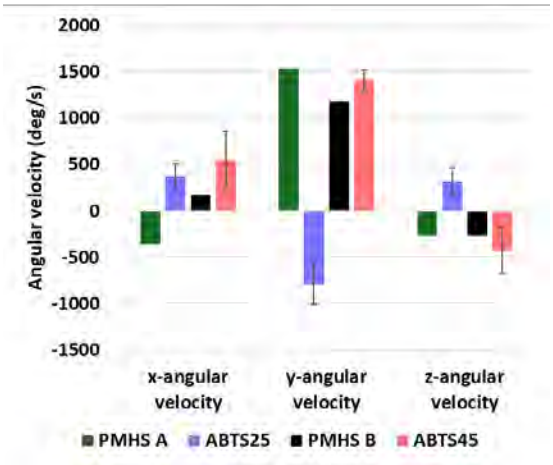

(a) Left iliac 6DOF block

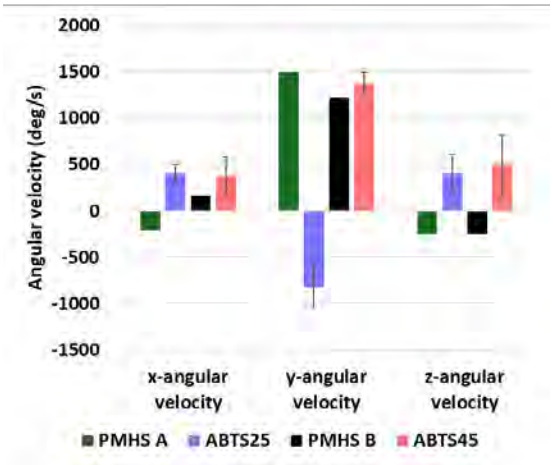

(b) Right iliac 6DOF block

Fig. C11. Pelvis angular velocity

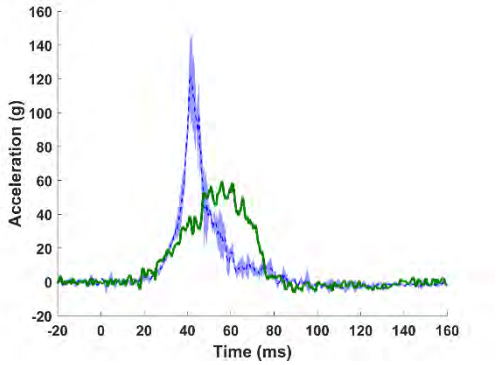

(a) Acceleration in x-direction (PMHS A)

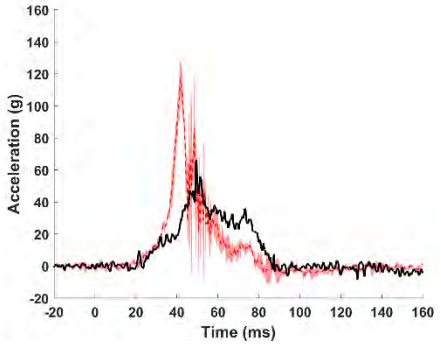

(b) Acceleration in x-direction (PMHS B)

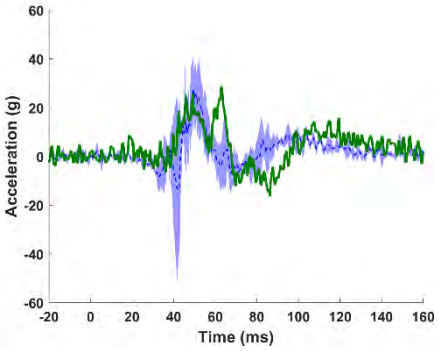

(c) Acceleration in z-direction (PMHS A)

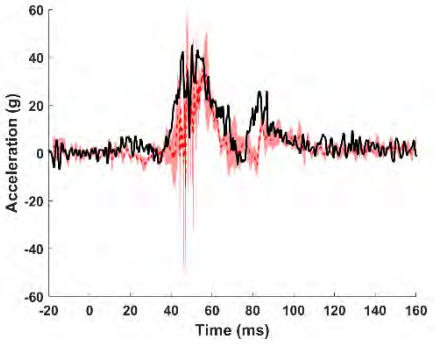

(d) Acceleration in z-direction (PMHS B)

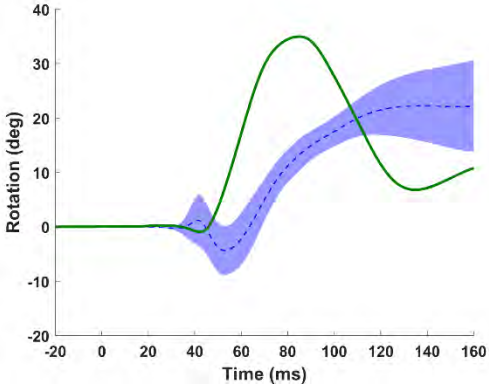

(e) Rotation about Y-axis (PMHS A)

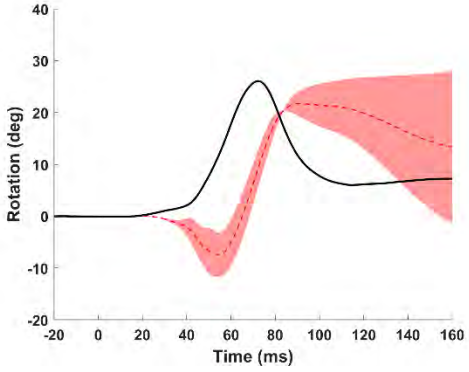

(f) Rotation about Y-axis (PMHS B)

Fig. C12. Pelvis linear acceleration in x- and z-directions and rotation about Y-axis measured from right iliac wing. Blue corridor: ABTS25 (N=3 [5]), red corridor: ABTS45 (N=3 [5]), green curve: PMHS A, black curve: PMHS B

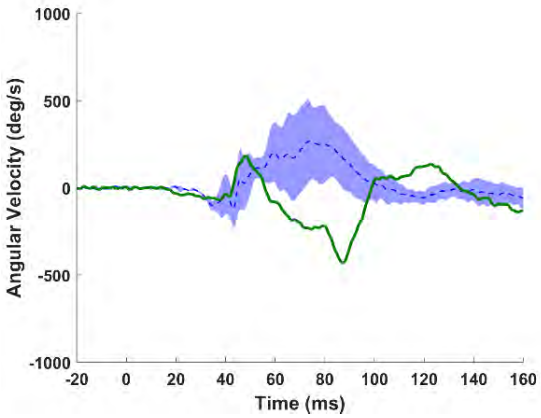

(a) Angular velocity about x-axis (Left)

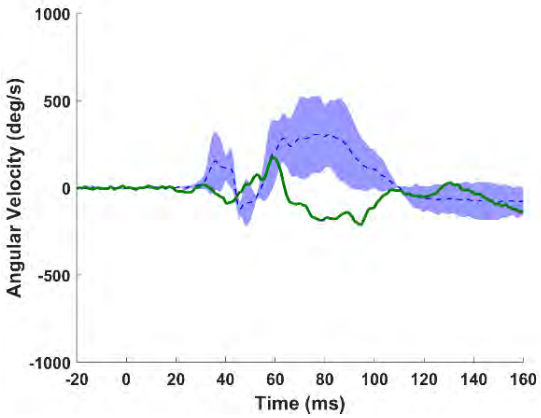

(b) Angular velocity about x-axis (Right)

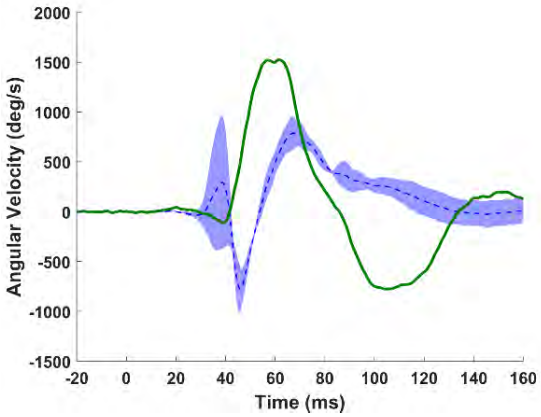

(c) Angular velocity about y-axis (Left)

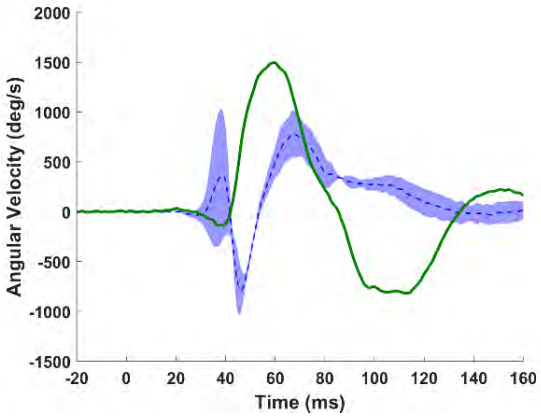

(d) Angular velocity about y-axis (Right)

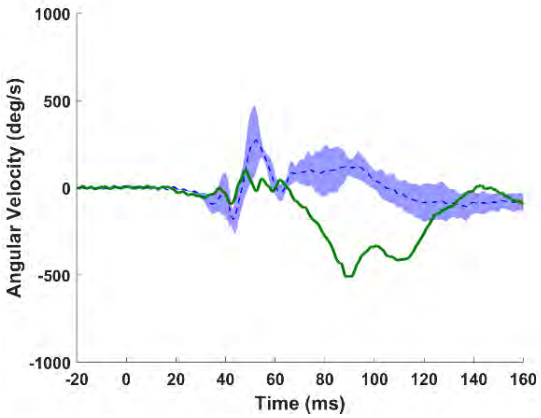

(e) Angular velocity about z-axis (Left)

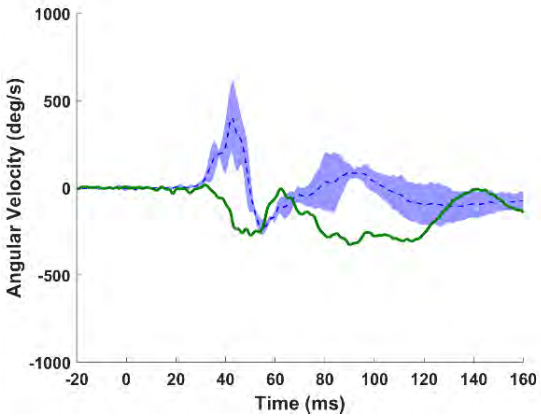

(f) Angular velocity about z-axis (Right)

Fig. C13. Pelvis angular velocity – PMHS A. Blue corridor: ABTS25 (N=3 [5]), green curve: PMHS A

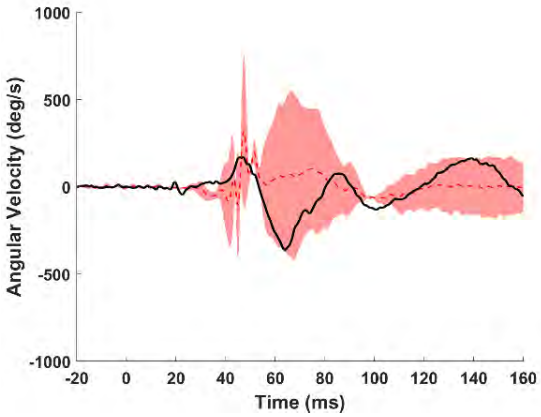

(a) Angular velocity about x-axis (Left)

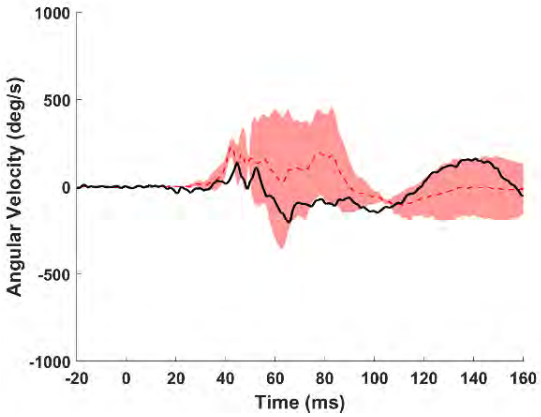

(b) Angular velocity about x-axis (Right)

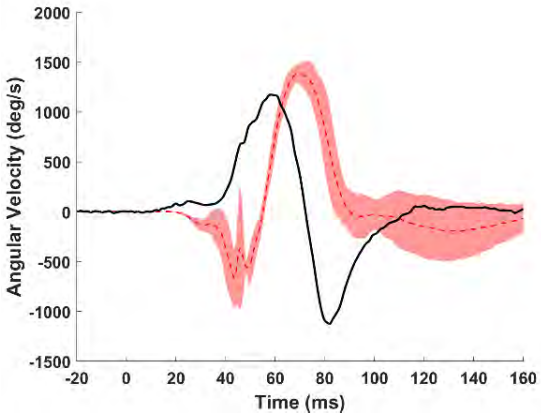

(c) Angular velocity about y-axis (Left)

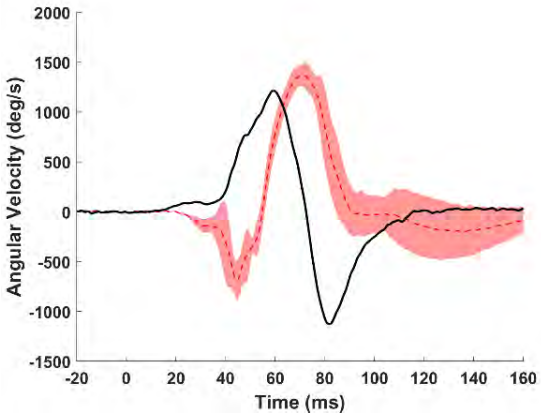

(d) Angular velocity about y-axis (Right)

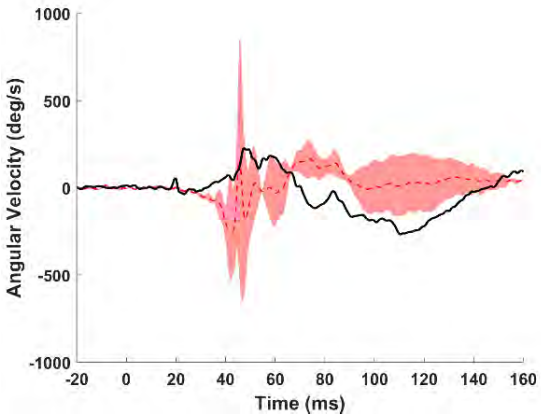

(e) Angular velocity about z-axis (Left)

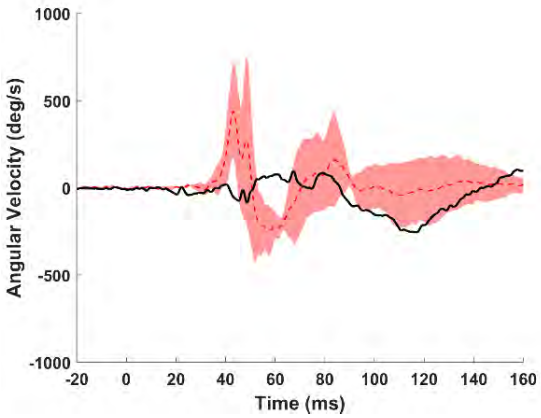

(f) Angular velocity about z-axis (Right)

Fig. C14. Pelvis angular velocity – PMHS B. Red corridor: ABTS45 (N=3 [5]), black curve: PMHS B

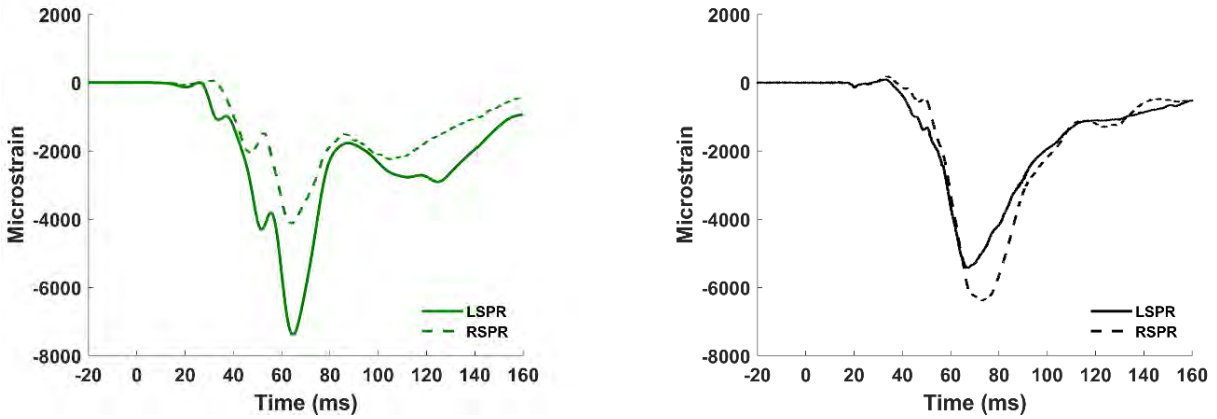

(a) PMHS A (LSPR: -7389μs & LSPR: -4126 μs) (b) PMHS B (LSPR: -5448μs & LSPR: -6391μs)

Fig. C15. Strain measured at left (LSPR) and right (RSPR) superior pubic rami. Unit: micro strain (μs)

Fig. C16. PMHS kinematics at the right clavicle fracture

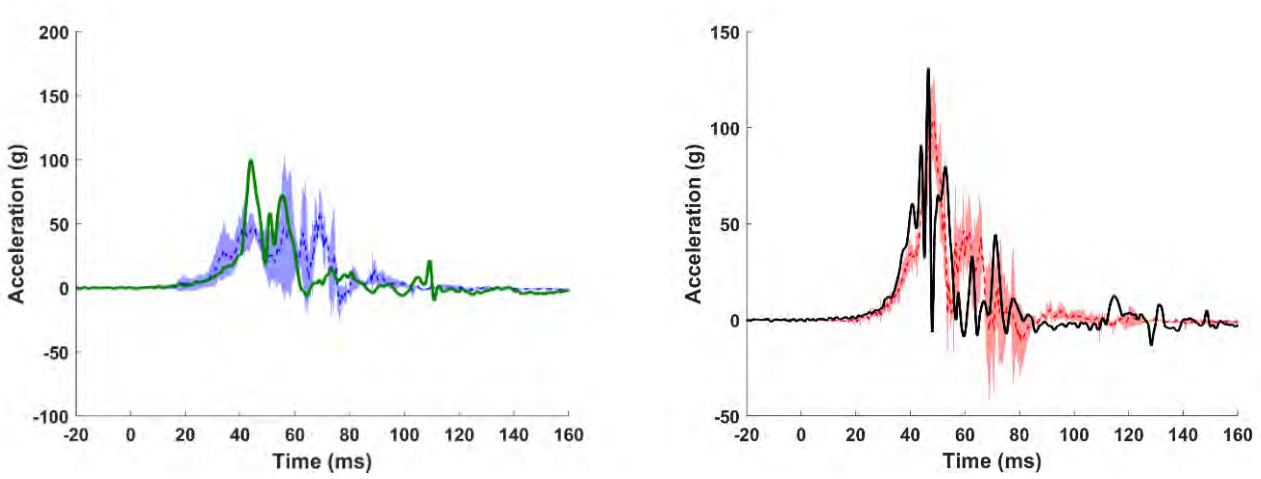

(a) PMHS A (b) PMHS B

Fig. C17. Right tibia acceleration in the x-direction. Blue corridor: ABTS25 (N=3 [5]), red corridor: ABTS45 (N=3 [5]), green curve: PMHS A, black curve: PMHS B